THEORETICAL MODELING AND EXPERIMENTAL VERIFICATION OF LASER DRILLING PROCESS OF SS316

M.Tech. Thesis

By

BITTU KUMAR

(2302103025)

DEPARTMENT OF MECHANICAL ENGINEERING

INDIAN INSTITUTE OF TECHNOLOGY INDORE

MAY 2025

THEORETICAL MODELING AND EXPERIMENTAL VERIFICATION OF LASER DRILLING PROCESS OF SS316

A THESIS

Submitted in partial fulfillment of the
requirements for the award of the degree
of
Master of Technology

by
BITTU KUMAR

DEPARTMENT OF MECHANICAL ENGINEERING
INDIAN INSTITUTE OF TECHNOLOGY INDORE
MAY 2025

INDIAN INSTITUTE OF TECHNOLOGY INDORE

CANDIDATE'S DECLARATION

I hereby certify that the work which is being presented in the thesis entitled **THEORETICAL MODELING AND EXPERIMENTAL VERIFICATION OF LASER DRILLING PROCESS OF SS316** in the partial fulfillment of the requirements for the award of the degree of **MASTER OF TECHNOLOGY** and submitted in the **DEPARTMENT OF MECHANICAL ENGINEERING,** Indian Institute of Technology Indore, is an authentic record of my own work carried out during the time period from June 2024 to May 2025 under the supervision of Dr. Dan Sathiaraj , Associate Professor , Department of Mechanical Engineering, IIT Indore and Dr. B.N. Upadhyaya, SOH, LTD, RRCAT Indore , Shri Vijay Kumar Bhardwaj, SOE, LTD, RRCAT Indore.

The matter presented in this thesis has not been submitted by me for the award of any other degree of this or any other institute.

Bittu Kumar
26-05-2025
Signature of the student with date
(Bittu Kumar)

This is to certify that the above statement made by the candidate is correct to the best of my/our knowledge.

26-05-25
Signature of the Supervisor of M.Tech. thesis
(Dr. Dan Sathiaraj)

Bnupadhyay
Signature of the Supervisor of M.Tech. thesis.
(Dr. B.N. Upadhyaya)

Vijay kumar
Signature of the Supervisor of M.Tech. thesis
(Shri Vijay Kumar Bhardwaj)

Bittu Kumar has successfully given his/her M.Tech. Oral Examination held on **9th May 2025**.

Bnupadhyay
Vijay kumar
26-05-25
Signature(s) of Supervisor(s) of M.Tech. thesis
Date: 26/05/2025

Convener, DPGC
Date: 28-5-25

ACKNOWLEDGEMENTS

First and foremost, I would like to express my deepest gratitude to my supervisor, Dr. B.N Upadhyaya, Dr. Dan Sathiaraj, and Shri Vijay Kumar Bhardwaj for their invaluable guidance, continuous support, and encouragement throughout the course of my research. Their expertise, insightful feedback, and patience played a vital role in the completion of this thesis. I am also sincerely thankful to the faculty and staff of IIT Indore and RRCAT Indore, whose dedication and assistance contributed greatly to my academic journey.

I would also like to extend my thanks to Prof. Suhas Joshi, Director of IIT Indore, and Prof. Shanmugam Dhinakaran, Head of the Mechanical Engineering Department, for their support and for providing the necessary research facilities during my research work. Additionally, The Teaching Assistantship (TA) provided by the Ministry of Human Resource Development (MHRD), Government of India, is also gratefully acknowledged.

Special thanks to Prabhat Kumar technician, RRCAT Indore, Pawan Kumar, scientific assistant, RRCAT Indore and Mr. Rajendra Goud PhD scholar, IIT Indore for their thoughtful discussions and technical support, which enriched the quality of this work. I would also like to acknowledge the support and understanding of my friends and colleagues, whose camaraderie made this journey more enjoyable and less daunting. Their presence and motivation were a constant source of strength.

Most importantly, I am deeply grateful to my family for their unconditional love, sacrifices, and unwavering belief in me. Without their support, this achievement would not have been possible.

Finally, I dedicate this work to all those who believed in me even during times I doubted myself. This thesis stands as a testament to their belief and encouragement.

Dedicated to my Parents, my sisters, teachers

and

loving memories of

Grandfather and Grandmother

Abstract

Laser drilling is a critical manufacturing process widely employed in aerospace, biomedical, and precision engineering sectors, especially for materials like SS316 stainless steel due to its excellent mechanical and corrosion-resistant properties. This study focuses on the development of a theoretical model and its experimental verification for optimizing the laser drilling process using a Fiber-coupled pulsed Nd: YAG laser of wavelength 1064nm. The primary objectives are to achieve maximum circularity, minimum taper angle, and increased depth of cut rate in the drilled holes. A comprehensive theoretical model was formulated based on laser-material interaction principles, considering energy absorption, thermal conduction, phase transformation, and recoil pressure-driven material ejection. Key process parameters such as laser pulse energy, pulse duration, repetition rate, beam diameter, number of pulses, assist gas pressure and focal position were integrated into the model to simulate their effect on hole quality and material removal efficiency. To validate the theoretical predictions, a series of controlled laser drilling experiments were performed on 3mm thick SS316 samples using a pulsed Nd: YAG laser system of wavelength 1064nm. Experimental outputs were measured using high-resolution optical microscopy to evaluate circularity, taper angle, and drilling depth. A comparative analysis between theoretical and experimental results was carried out, revealing a high degree of agreement, particularly in predicting the hole geometry and drilling efficiency trends. The developed model proved to be a powerful predictive tool for process optimization, reducing the need for extensive trial-and-error experimentation. This work not only contributes to the understanding of pulsed laser drilling dynamics but also offers practical guidelines for precise micro-machining of stainless-steel components.

TABLE OF CONTENTS

LIST OF FIGURES……………………………………………………………...............xi

LIST OF TABLES…………………………………………………………….....xiii

NOMENCLATURE……………………………………………………………...xv

ACRONYMS……………………………………………………………….xvii

Chapter 1: Introduction……………………………………………………...1-23

1.1 Introduction of laser…………………………………………………...1

1.1.1 Working principle of laser…………………………………….................2

1.1.2 Types of lasers…………………………………………………........6

1.1.2.1 Introduction to gas lasers……………………………………………......7

1.1.2.1.1 Introduction to carbon dioxide (CO_2) laser…………………….................7

1.1.2.1.2 Introduction to CO laser………………………………………………9

1.1.2.1.3 Introduction to He-Ne laser…………………………………………......10

1.1.2.2 Introduction to liquid(dye) laser……………………………………...10

1.1.2.3 Introduction to Solid-state laser……………………………………………11

1.1.2.3.1 Neodymium–doped Yttrium Aluminium Garnet Lasers (Nd: YAG) ………...12

1.1.2.3.2 Introduction to semiconductor laser …………………………………14

1.1.2.3.3 Introduction to Nd: Glass laser……………………………………......15

1.1.2.3.4 Introduction to Fiber laser……………………………………….....15

1.1.3 Laser safety and hazardous…………………………………………16

1.2 Introduction to laser cutting……………………………………………...17

1.2.1 The process of laser cutting………………………………………………17

1.3 Introduction to laser drilling……………………………………………...18

1.3.1 Advantage of laser drilling………………………………………………..19

1.3.2 Types of laser drilling……………………………………………………..19

1.3.2.1 Single pulse drilling……………………………………………………19

1.3.2.2 Percussion drilling…………………………………………………....20

1.3.2.3 Trepanning……………………………………………………………21

1.3.2.4 Helical trepanning……………………………………………………22

1.4 Overview of workpiece material SS316………………………………...23

Chapter 2: Literature Survey, Objectives and Methodology…………………………25-30

2.1 Objectives of the study…………………………………………………27

2.2 Problem statement……………………………………………………………..28
2.2 Problem statement……………………………………………………………..29
Chapter 3: Experimental Investigations…………………………………………..31-50
3.1 Laser material interaction……………………………………………………...31
3.2 Experimental setup……………………………………………………………33
3.3 Experimental details…………………………………………………………...34
3.4 Taguchi method………………………………………………………………..34
3.5 Optimization of laser drilling process…………………………………………37
3.5.1 Maximization of hole circularity………………………………………………38
3.5.2 Minimization of taper angle of hole…………………………………………...44
Chapter 4: Theoretical Modeling………………………………………………51-56
4.1 Model description……………………………………………………………...51
4.2 Assumptions…………………………………………………………………51
4.3 Aim of model…………………………………………………………………..51
4.4 Mathematical formulation……………………………………………………..51
4.4.1 Mass balance…………………………………………………………………..51
4.4.2 Melt ejection velocity…………………………………………………………52
4.4.4 Assist gas pressure……………………………………………………………..53
4.4.6 Energy balance………………………………………………………………53
4.5 Physical properties……………………………………………………………..53
4.6 Results and discussions………………………………………………………...54
Chapter 5: Experimental verification…………………………………………...57-58
5.1 Experimental description……………………………………………………57
5.2 Formulation and calculation…………………………………………………57
5.3 Results and discussions………………………………………………………58
Chapter 6: Conclusion………………………………………………………………....59
REFERENCES…………………………………………………………………………....61

LIST OF FIGURES

Fig.1.1 Schematic diagram of Laser light generation……………….…………………1
Fig.1.2 Absorption of energy by atom….……………………………………………...3
Fig.1.3 Energy diagram for absorption………………………………………...…3
Fig.1.4 The phenomena of spontaneous emission……………………………............4
Fig.1.5 The phenomena of stimulated emission…………………………………..........6
Fig.1.6 Schematic diagram of CO_2 laser………………………………………………8
Fig.1.7 Image of CO_2 laser setup at IITI……………………….………………...8
Fig.1.8 Image of Nd: YAG laser setup at IITI…….……………………………...12
Fig.1.9 Schematic diagram of four level energy laser…………………………………14
Fig.1.10 Image of Fiber laser setup at IITI….…………………………………………..16
Fig.1.11 Schematic diagram of laser cutting/drilling setup…………………………..18
Fig.1.12 Schematic diagram of single pulse laser drilling…………………………………20
Fig.1.13 Schematic diagram of laser percussion drilling………………………………..21
Fig.1.14 Schematic diagram of trepanning…………………………………………...22
Fig.1.15 Schematic diagram of helical trepanning…………………………………………23
Fig.3.1 Laser material interaction diagram………………………………………………..31
Fig.3.2 Laser material processing parameters……………………………………………..32
Fig.3.3 Level of intensity required for different phenomena……………………………...32
Fig.3.4 Schematic diagram of laser drilling setup…………………………………………33
Fig.3.5 250 W average power and 5kW peak power industrial Nd:YAG laser with multi-port Fiber optic beam delivery at RRCAT, Indore.……………………….……………………33
Fig.3.6 Image of laser drilled sample top side……………………………………………..34
Fig.3.7 Image of laser drilled sample bottom side…………………………………………34
Fig.3.8 Closure view of laser drilled hole top side……………….………………………...34
Fig.3.9 Closure view of laser drilled hole bottom side……………….…………………….34
Fig.3.10 S/N ratio vs number of pulses……………………………………………………41
Fig.3.11 S/N ratio vs pulse width……………………………………...……………...40
Fig 3.12 S/N ratio vs repetition rate…...…………………………………………………42
Fig.3.13 S/N ratio vs peak power……………………………………...……………...42
Fig 3.14 S/N ratio vs assist gas pressure………………..………………………………44
Fig.3.15 Microscope image of front hole diameter and back hole diameter…………………46
Fig.3.16 S/N ratio vs number of pulses………….……………………………………..48
Fig.3.17 S/N ratio vs pulse width…………………………………………………………..48

Fig3.18 S/N ratio vs repetition rate……………………..………………………………49

Fig.3.19 S/N ratio vs peak power…………………..……………………………………...49

Fig.3.20 S/N ratio vs assist gas pressure……………..……………………………………50

Fig.4.1 Absorbed laser intensity vs melt surface temperature……………………………..55

Fig 4.2 Absorbed laser intensity vs melt ejection velocity………………………………..56

Fig.5.1 Comparison of theoretical data with experimental data…………………………..58

LIST OF TABLES

Table 1: Selection of orthogonal array……………………………………………………….37

Table 2: Factors and levels……………………………………………………………...37

Table 3: L_{16} Taguchi orthogonal array……………………………………………………….38

Table 4: Experimental data for maximum hole circularity………………………………..39

Table 5: Experimental levels and data analysis for Table 4……………………………….39

Table 6: Mean S/N value for each level and factor for maximum hole circularity………..41

Table 7: Experimental data for minimum taper angle……………………………………..45

Table 8: Experimental levels and data analysis for Table 7……………………………......45

Table 9: Mean S/N value for each level and factor for minimum taper angle……………..47

Table 10: Theoretical calculation at varying melt surface temperatures…………………….54

Table 11: Experimental calculated data……………………………………………………...57

NOMENCLATURE

A	Coefficient of absorption
A_e	Effective area of assist gas flow
A_r	Cylindrical area of radial loss assist gas pressure
D_f	Front diameter
D_b	Back diameter
h	Planck’s constant
I_{abs}	Absorbed laser intensity
υ	frequency
L_V	Latent heat of vaporization
m_s	Mass of solid metal melted
m_v	Mass of molten metal vapourised
m_m	Mass of molten material ejected
α	Taper angle in degree
ρ_s	Density of solid
ρ_m	Density of melt
δ_m	Melt thickness
M_A	Atomic mass
N_A	Avogadro's number
p_r	Recoil pressure
p_{eff}	Assist gas effective pressure
p_{vap}	vapour pressure
p_{atm}	Atmospheric pressure
p_g	Pressure of assist gas at nozzle exit
p_n	Pressure inside the nozzle
P_L	Incident laser power
P_R	Reflected laser power
R	Coefficient of reflectivity
r_l	Laser beam radius
T_s	Melt surface temperature
T_{vap}	Temperature of vaporization

V_d	Drilling velocity along z-axis
V_v	Vaporization front velocity
V_m	Melt ejection velocity
y_i	Observed data (or quality characteristics) at *i*th trial

ACRONYMS

Avg.	Average
cm	Centimeter
CNC	Computer numerical control
He-Ne	Helium-Neon
HAZ	Heat-affected zone
Kg	Kilogram
kW	Kilowatt
mm	Millimeter
ms	Millisecond
µm	micrometer
MW	Megawatt
Nd: YAG	Neodymium-doped Yttrium Aluminium Garnet
SS	Stainless steel
SN	Signal to noise

Chapter 1

Introduction

1.1 **Introduction of Laser:** It is an acronym of **Light Amplification by Stimulated Emission of Radiation**. It is a powerful device that emits a beam of light that is coherent, monochromatic, and highly directional beam of light [1]. The unique properties of laser light is its coherence, directionality, and single wavelength arising from its underlying physical principles, which distinguish it from ordinary light sources. Essential Components of a Laser are gain/active medium, pumping source (energy source) and optical resonator (cavity) [1]. Figure 1.1 shows the schematic of laser light generation.

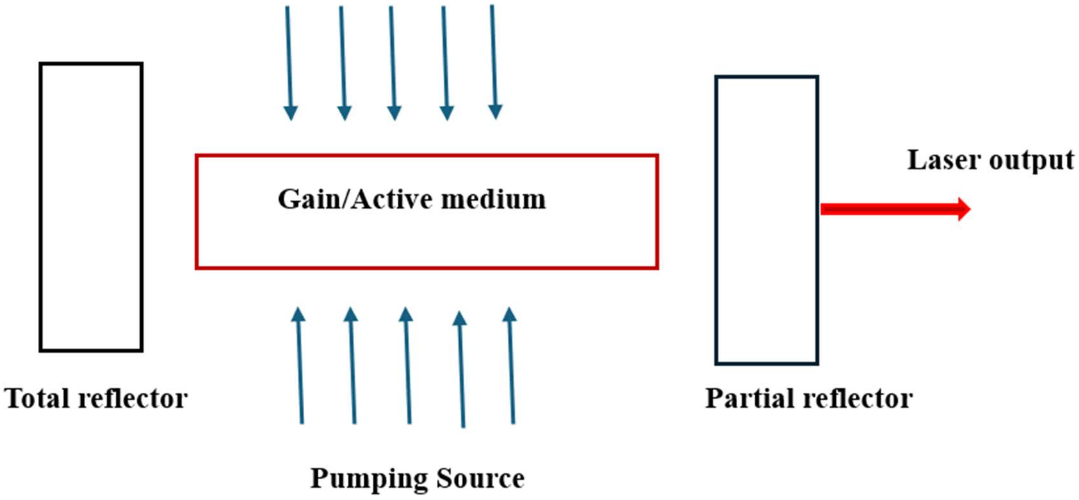

Fig. 1.1: Schematic diagram of laser light generation.

Gain/Active medium: The gain medium is the important part of the laser. It is the material where light amplification occurs through stimulated emission. It can be in various physical states: solid, liquid, gas or plasma [1].

Gas lasers: e.g., Helium-Neon (He-Ne), CO_2 lasers.

Solid-state lasers: e.g., Ruby, Nd: YAG.

Liquid dye lasers: Using organic dyes dissolved in solvents.

Semiconductor lasers: e.g., laser diodes, used in Fiber optics and electronics.

The active medium defines the wavelength of the laser and significantly influences its power and application range [1].

Pumping source: To achieve population inversion, energy must be supplied to the gain medium through a process called pumping. The common methods for pumping are:

Electrical Discharge: It is used in gas lasers.

Flash Lamps or Arc Lamps: It is used in solid-state lasers.

Laser Diode Pumping: It is Efficient and commonly used for compact systems.

Chemical Reaction or Nuclear Pumping: It is used in specialized lasers.

Optical Resonator: The optical resonator comprises of two mirrors placed at opposite ends of the gain medium. It plays an important role in amplifying the emitted light:

High Reflector: A high reflector is an optical mirror with nearly 100% reflectivity, for the specific wavelength of the laser being produced. It is positioned at one end of the laser cavity [1].

Output Coupler: The Output Coupler is one of the two mirrors that make up the optical resonator (or laser cavity) in a laser. It is partially reflective, allowing a controlled fraction of the amplified light to escape the cavity as the usable laser output. It plays an important role in balancing laser gain and output efficiency [2].

1.1.1 **Working Principle of a Laser:** It is based on the quantum mechanical process of stimulated emission, enabled by achieving population inversion in an active medium and amplifying light within an optical resonator. This results in the emission of a coherent, monochromatic, and highly directional beam of light, which forms the basis for the diverse applications of lasers in science, industry, medicine, and technology. The operation of a laser is governed by several key physical processes at the atomic level. These includes absorption, spontaneous emission, stimulated emission and population inversion.

Absorption: It is a fundamental physical process in which atoms or molecules take up energy from electromagnetic radiation, typically light, resulting in a transition of electrons from a lower energy state (ground state) to a higher energy state (excited state). This process is called absorption and is the first step in the laser process [1, 2]. Figure 1.2 shows absorption of energy by atom and figure 1.3 shows energy diagram for absorption.

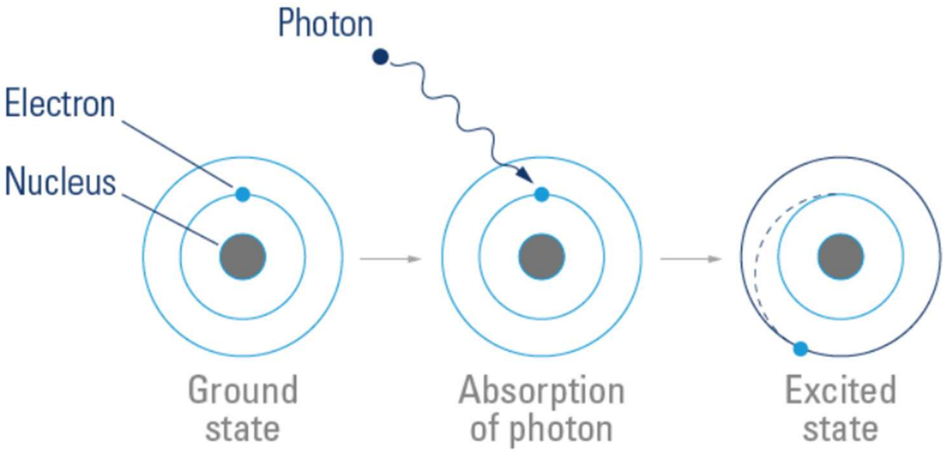
Photon
Electron
Nucleus
Ground state
Absorption of photon
Excited state

Fig. 1.2: Absorption of energy by atom.

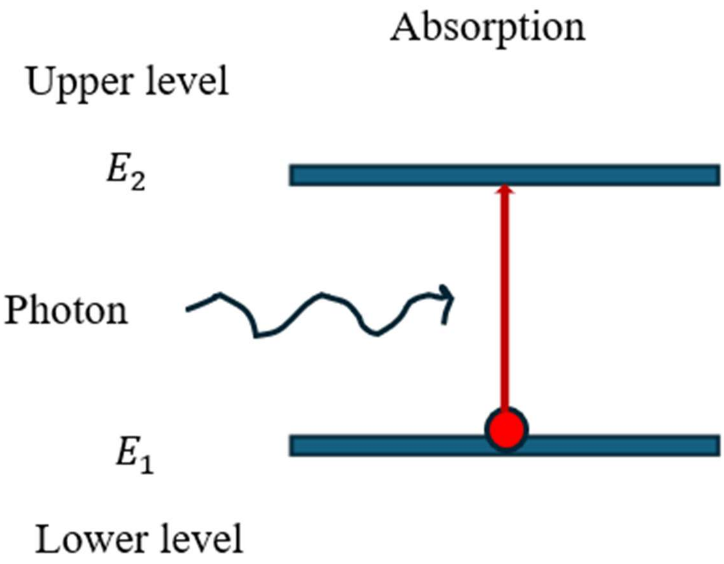
Absorption
Upper level
E_2
Photon
E_1
Lower level

Fig. 1.3: Energy diagram for absorption.

Principle of absorption:

Unique Wavelengths: Each element has a unique electronic structure, meaning its atoms or ions absorb light at specific, characteristic wavelengths. When exposed to light of these precise wavelengths, only the atoms of that element will absorb the energy, causing their electrons to move from the ground state to an excited state.

Energy Transition: The absorption of a photon corresponds to the energy difference between two discrete energy levels in the atom or molecule. The process can be represented as follows:

$$E_{photon} = h\upsilon = E_{excited} - E_{ground} \qquad [1]$$

Where h is Planck's constant.

Spontaneous emission: Excited electrons are unstable and tend to return to their lower energy (ground) state. When they do so without external influence, they emit a photon randomly in phase and direction. This process is called spontaneous emission and is responsible for incoherent light sources like fluorescent lamps. This process is fundamental to understanding light-matter interactions and underpins phenomena such as fluorescence, phosphorescence, and laser operation. Spontaneous emission cannot be explained classically and requires quantum electrodynamics [1]. Figure 1.4 shows the phenomena of spontaneous emission.

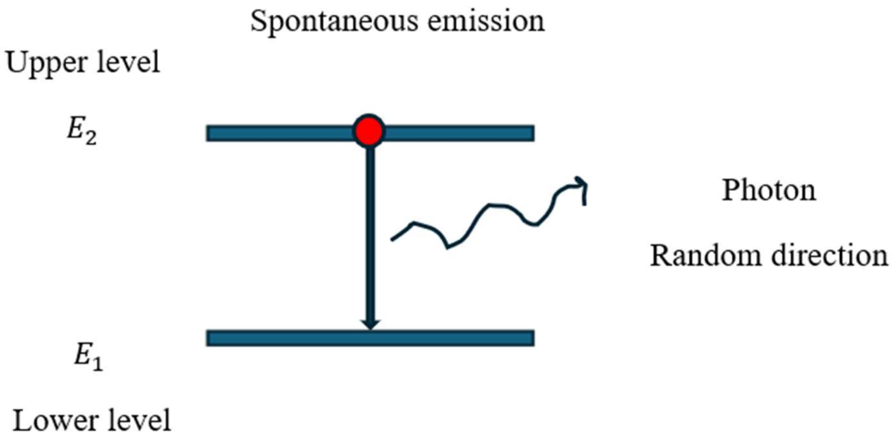

Fig. 1.4: The phenomena of spontaneous emission.

Key characteristics:

Random direction and phase: Spontaneously emitted photons exhibit random direction and phase due to fundamental quantum mechanical principles and practical experimental conditions. As emitted photons propagate in random directions and have uncorrelated phases, resulting in incoherent light (e.g., from lamps or LEDs) [2].

Intrinsic decay mechanisms: The intrinsic decay mechanism refers to the natural, unavoidable process by which an excited quantum system (such as an atom, molecule, or ion) transits from a higher energy state to a lower energy state, emitting a photon in the process. This phenomenon is known as spontaneous emission and is fundamentally rooted in quantum mechanics. It occurs naturally in excited systems due to their instability, with the decay time governed by the spontaneous emission lifetime (ranging from nanoseconds to seconds) [3].

Stimulated emission: It is a quantum mechanical process in which an incoming photon of a specific energy interacts with an atom or molecule that is already in an excited energy state, causing it to drop to a lower energy state and emit a second photon. The emitted photon has the same energy (frequency), phase, direction, and polarization. When an atom or molecule is in an excited state, it can return to a lower energy state either spontaneously or by interacting with an external photon. If a photon with energy exactly equal to the energy gap between the excited and lower state passes by, it can trigger the excited atom to emit a second photon as it returns to the lower state. The emitted photon is an exact clone of the incident photon: it travels in the same direction, has the same frequency, phase, and polarization. When a population inversion is achieved (more atoms in the excited state than in the ground state), stimulated emission dominates over absorption, allowing for a chain reaction of photon emission and the build-up of a coherent, intense light beam. Figure 1.5 shows the phenomenon of stimulated emission.

Mathematically, the rate of stimulated emission is directly proportional to the number of atoms in excited state, the energy density of the incident photons and the Einstein coefficient, which characterizes the probability of stimulated emission for a particular transition.

The rate of stimulated emission = $-B_{21}N_2\rho(\upsilon)$ [2]

Where, B_{21}= The Einstein coefficient for this process, N_2 = Number of atoms in excited state, $\rho(\upsilon)$ = The energy density of the field or the electromagnetic energy density

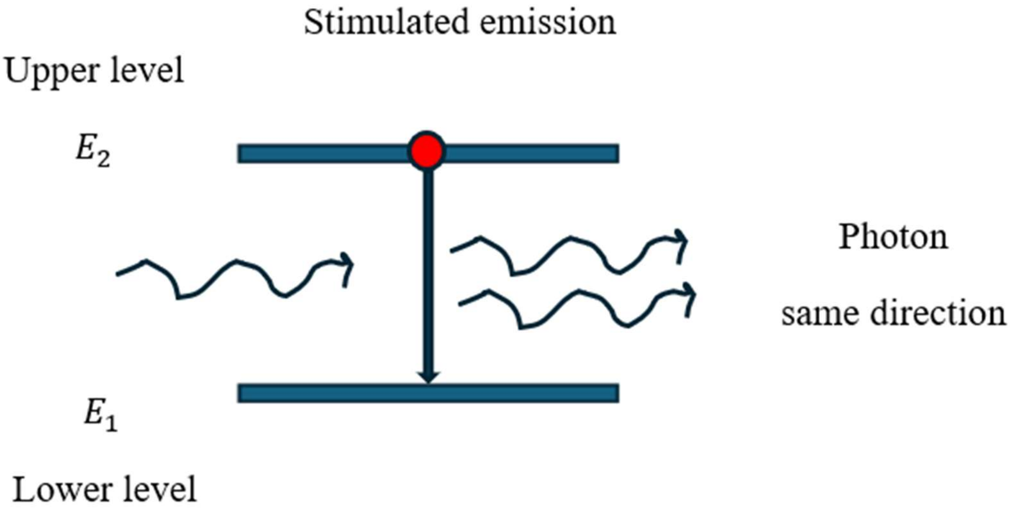

Fig. 1.5: The phenomena of stimulated emission.

Population inversion: It is a fundamental concept in laser technology, describing a non-equilibrium condition where more atoms or molecules occupy a higher energy state than a lower one within a given system. This state is essential for the operation of lasers. Under the normal conditions, most atoms reside in the ground (i.e. lowest energy) state, as dictated by the Boltzmann distribution. The population of higher energy state is always less than that of lower energy state. But in population inversion, the normal order is reversed and the number of atoms in an excited (higher energy) state exceeds those in a lower (often ground) state.

Mathematically, if N_2 is the population of the excited state and N_1 is of the ground state, then the condition for population inversion is $N_2 > N_1$.

1.1.2 **Types of lasers:** Lasers are classified based on the nature of their active medium that means the material in which light amplification occurs. Each type of laser offering unique properties such as wavelength range, power, and tunability. The wavelength of a laser is decided by the energy difference as the excited atoms or molecules are stimulated to a lower energy level [1]. This diversity of laser enables lasers to serve a vast array of scientific, industrial, medical, and consumer applications [1, 5]. Some important types of lasers are gas lasers, liquid/dye lasers, semiconductor (diode) lasers, Fiber lasers and solid-state lasers.

1.1.2.1 **Introduction to Gas lasers:** Gas lasers represent a significant category of lasers that utilize gases or a blend of gases as the gain medium. These lasers are extensively utilized in scientific, industrial, and medical applications because of their capacity to generate coherent, high-quality beams over various wavelengths. Gaseous substances or mixtures are energized through an electrical discharge [1, 5].

Working principle of Gas lasers: Gas lasers working is based on the concept of stimulated emission. The active or gain medium is generally a gas or a combination of gases (such as helium and neon, argon and nitrogen, or carbon dioxide) housed within a glass tube. An external energy source, typically an electric discharge, energizes the gas atoms or molecules, moving them to higher energy levels. When these excited particles transition back to lower energy states, they release photons. If the circumstances are favourable, these photons can initiate additional emissions, resulting in a cascading effect and the amplification of light within a resonant optical cavity created by mirrors located at both ends of the tube [1, 5].

Types of Gas laser: Gas lasers are classified according to the characteristics of their active medium and the specific atomic or molecular transitions that take place. There are some important types of Gas lasers i.e., carbon dioxide(CO_2) laser, carbon monoxide (CO) laser, Helium-neon (He-Ne) laser, Argon-ion laser and Krypton-ion laser.

1.1.2.1.1 Introduction to Carbon dioxide(CO_2) laser: A carbon dioxide laser is a gas laser that utilizes a mixture of gases, mainly carbon dioxide (CO_2), nitrogen (N_2), and helium (He), as its active medium [1]. The construction of carbon dioxide laser contain important parts such as discharge tube, electrodes, Mirrors, cooling systems, optical elements and gas circulation.

Working principles of CO_2: The CO_2 laser functions as a four-level molecular gas laser, with the laser process taking place between the vibrational-rotational energy states of CO_2 molecules. A high-voltage electric discharge excites the nitrogen molecules in the gas mixture. Nitrogen is chosen because its excited vibrational energy level matches that of CO_2, allowing efficient energy transfer. Enthusiastic N_2 molecules impact CO_2 molecules, exchanging energy and promoting CO_2 to higher vibrational states, resulting in a population inversion. When the energized CO_2 molecules transition back to a lower vibrational state, they release photons in the infrared spectrum primarily at 10.6µm wavelength. The released photons ricochet between the mirrors, prompting additional emission and enhancing the light inside the resonator. The semi-reflective mirror permits a segment of the intensified light to escape as a strong, coherent laser beam.

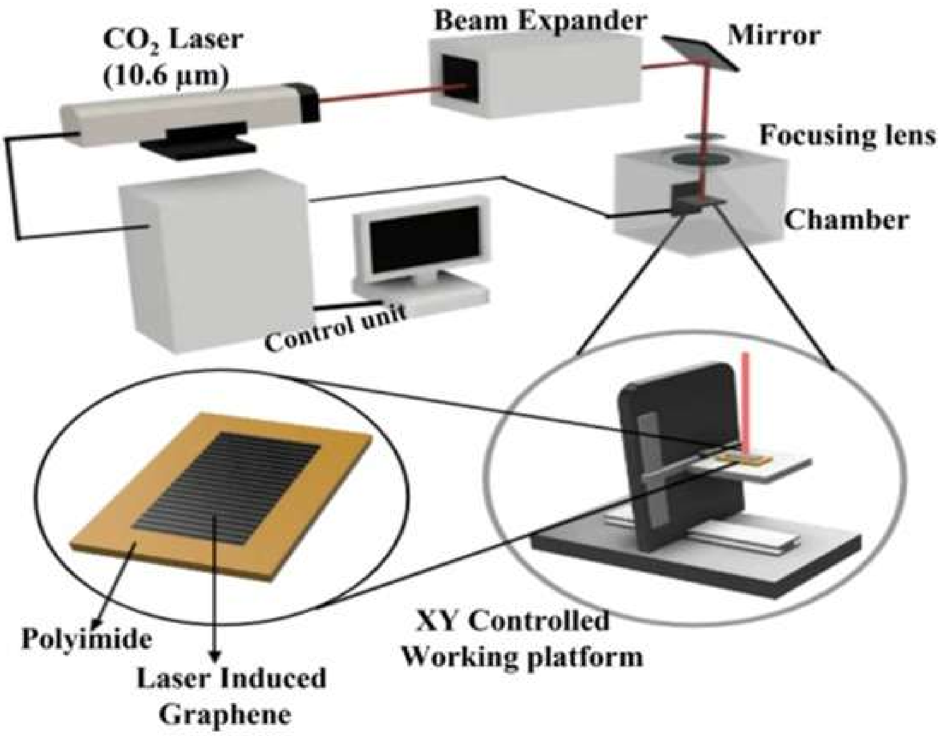
CO_2 Laser
(10.6 µm)
Beam Expander
Mirror
Focusing lens
Chamber
Control unit
Polyimide
Laser Induced Graphene
XY Controlled Working platform

Fig. 1.6: Schematic diagram of CO_2 laser.

LASER µ3D PRINTER
DST/TDT/AMT/2017/131

Fig. 1.7: Image of CO_2 laser setup at IITI.

Applications of CO_2 laser: CO_2 lasers rank among the most commonly utilized lasers in both industrial and medical applications because of their excellent efficiency and adaptability.

Industrial Applications: Machining and joining metals, plastics, textiles, and various other substances. Engraving and marking on materials such as wood, acrylic, leather, and beyond. Selective laser sintering utilized in 3D printing and production etc [1, 5].

Medical Applications: Surgical interventions include soft-tissue surgery, tumour excision, gynaecological procedures, ENT treatments, and dental surgeries. Procedures for improving skin texture, eliminating wrinkles, and addressing various skin issues. Procedures for improving skin texture, eliminating wrinkles, and addressing various skin issues, etc. [1, 5].

The non-contact functionality of CO_2 laser decreases tool wear. It offers high speed and precision. There is minimal thermal damage to adjacent materials. It demonstrates versatility across a broad spectrum of materials [5].

1.1.2.1.2 Introduction to CO laser: Carbon monoxide (CO) lasers are a type of gas laser that produces radiation in the mid-infrared range, generally between 4.8 µm and 8.3 µm. These lasers utilize a mixture of gases that includes carbon monoxide (CO), nitrogen (N_2), helium (He), and occasionally hydrogen (H_2) or xenon (Xe). An electrical discharge excites the CO molecules, energizing the nitrogen molecules. Subsequently, these energized nitrogen molecules transfer their energy to CO molecules via collisions, establishing the population inversion needed for laser operation. The laser emission results from transitions between vibrational-rotational energy states in CO molecules, with multiple spectral lines present across its range of operation.

CO lasers achieve impressive wall-plug efficiencies of up to 40%, significantly surpassing the typical 10-20% efficiencies seen in CO_2 lasers. This high efficiency, along with their shorter infrared wavelengths (in contrast to the 9-11 µm range of CO_2 lasers), makes CO lasers especially suitable for precise material processing applications, such as cutting glass and plastics, where their radiation is absorbed more effectively. They are also utilized in various medical procedures, scientific research, and laser absorption spectroscopy. The design consists of a gas discharge tube with mirrors at either end—one completely reflective and the other partially transparent to allow the emission of the laser beam—along with cooling systems to handle the heat generated during operation. Despite their benefits, CO lasers have historically struggled with longevity issues, although recent developments have enhanced their reliability for both industrial and medical uses.

1.1.2.1.3 Introduction to He-Ne laser: A Helium-Neon (He-Ne) laser is a type of gas laser that utilizes a combination of helium and neon gases, generally in a ratio of about 10:1, contained at low pressure within a glass tube. When a high-voltage electrical discharge is applied to the electrodes located at both ends of the tube, energetic electrons elevate helium atoms to higher energy levels. These excited helium atoms then transfer their energy to neon atoms through collisions, which selectively excite the neon atoms to specific metastable states. This process generates a population inversion in the neon atoms, which is crucial for laser operation. The lasing action occurs when neon atoms transition from a higher metastable state to a lower energy state, releasing coherent red light at a wavelength of 632.8 nm. The laser cavity, created by mirrors at each end of the tube—one fully reflective and the other partially transmitting—ensures that photons bounce back and forth, promoting further emissions and amplifying the light. The result is a stable, highly coherent, and monochromatic red beam, widely utilized in scientific research, metrology, holography, alignment, and medical applications due to its reliability and precision.

1.1.2.2 **Introduction to liquid(dye) laser: A** liquid or dye laser is a kind of laser that produces light across a wide and adjustable range of wavelengths, frequently from the ultraviolet to the near-infrared regions, by dissolving an organic dye in a liquid solvent (such as water, alcohol, or ethylene glycol) as its active lasing medium. Usually, a dye cell or jet circulates the dye solution, which is then optically pumped—typically by a flashlamp or another laser—to excite the dye molecules to higher energy states. As the molecules return to lower energy states, they emit light via stimulated emission, which is amplified by mirrors creating a resonant cavity.

Dye lasers are useful for spectroscopy, medicine, and research because of their broad wavelength tunability (up to 50–100 nm or more with a single dye, and even wider with multiple dyes), high efficiency (up to 25–30% for laser pumping), and capacity to produce ultrashort pulses. Using wavelength-selective components such as prisms or diffraction gratings inside the resonator, the output wavelength can be precisely chosen. Common dyes include coumarin, fluorescein, and rhodamine 6G. However, compared to many other laser types, dye lasers are typically more costly and technically hard to operate, and they need sophisticated circulation systems to prevent dye degradation and triplet state absorption.

Dye or liquid lasers can be divided according to their operation mode and the specific dye utilized as the lasing medium. The primary types of operation are continuous-wave (CW) dye lasers, which offer a consistent and stable output that is perfect for high-resolution spectroscopy and atomic cooling, and pulsed dye lasers, which emit powerful, brief flashes of light ideal for applications like medical treatments and rapid spectroscopy. The selection of dye affects the efficiency and wavelength range: popular dyes consist of Rhodamine 6G (570–650 nm, yellow orange), Coumarin dyes (blue-green, 450–510 nm), and Stilbene dyes (near-UV, approximately 400 nm). Dye lasers are additionally categorized based on their cavity and resonator architectures, including linear, ring, or narrow-linewidth designs, which facilitate precise wavelength selection using components such as diffraction gratings and prisms. Beyond the conventional liquid form, there are solid-state dye lasers where the dye is incorporated into a solid organic matrix. This adaptability makes dye lasers exceptionally tuneable across a wide range of wavelengths, supporting numerous scientific, medical, and industrial uses.

1.1.2.3 **Introduction to Solid-state laser:** Typically, a crystal or glass doped with rare-earth or transition metal ions like neodymium (Nd^{3+}), chromium (Cr^{3+}), or ytterbium (Yb^{3+}) serves as the gain (active) medium for a solid-state laser [1, 6]. This sets them apart from dye lasers, which use liquids, and gas lasers, which use gasses. To create a population inversion, the laser uses the stimulated emission method, which involves providing energy (often through optical pumping) to excite the dopant ions in the solid medium. These ions release photons upon returning to their ground state, and an optical resonator amplifies these photons to create a coherent laser beam. Compared to gas lasers, solid-state lasers can store more energy due to their relatively lengthy excited state lifetimes. This enables them to be Q-switched to produce extremely high peak powers in brief bursts [1].

Different types of solid-state lasers are distinguished by the host materials and dopant ions that are employed as the gain medium. The most popular are semiconductor lasers and neodymium-doped lasers, which are usually found in the near-infrared spectrum and offer high power, efficiency, and excellent beam quality. Examples of these include neodymium-doped yttrium aluminium garnet (Nd: YAG), neodymium glass lasers (Nd: Glass), and diode-pumped solid-state lasers. Furthermore, Fiber lasers are regarded as a subclass of solid-state lasers and are distinguished by their high power, efficiency, and beam quality. These lasers use rare-earth-doped optical Fibers as the gain medium. Each kind of solid-state laser is designed for a particular use based on its efficiency, tunability, and output properties.

1.1.2.3.1 **Neodymium–doped Yttrium Aluminium Garnet Lasers (Nd: YAG):** A common solid-state laser, the Nd: YAG laser (Neodymium-doped Yttrium Aluminum Garnet laser) uses a synthetic Yttrium Aluminum Garnet (YAG) crystal doped with neodymium ions (Nd^{3+}) as its active medium. Its primary wavelength of light emission is 1064 nm, which is in the near-infrared spectrum [1, 6].

It delivers high output power alongside elevated repetition rates. It is suitable for both continuous and pulsed operations, featuring Q-switching for extremely short, high-intensity pulses. It can effectively process highly reflective materials, such as aluminium and copper, which can be difficult for other laser types. The beam quality is exceptional and offers high precision. It is relatively straightforward to operate and maintain, and its purchasing costs are lower compared to other laser types. It is adaptable for a variety of applications, ranging from fine marking to deep cutting.

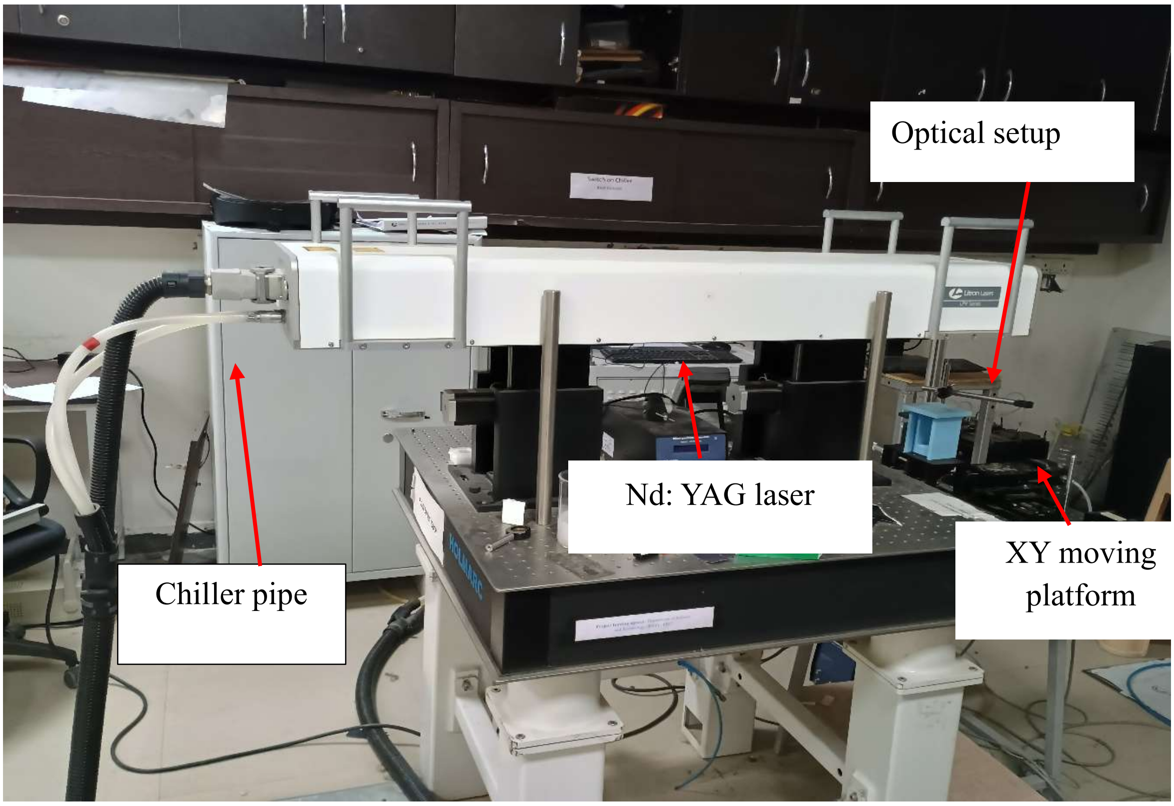

Fig. 1.8: Image of Nd: YAG laser setup at IITI.

The Nd: YAG laser consists of three primary components:

Active Medium: At the canter of the laser is a rod-shaped crystal made of YAG that's been doped with approximately 1.5% neodymium ions. This rod serves as the gain medium where the lasing process takes place.

Energy Source (Pump Source): Optical pumping is usually achieved using either a krypton or xenon flash lamp, or laser diodes. The pump source is positioned next to the Nd: YAG rod, typically within an elliptical reflector cavity to optimize light transfer into the rod.

Optical Resonator: The rod is located between two mirrors—one that is fully reflective (total reflector) and another that is partially reflective (output coupler). These mirrors create the resonant optical cavity, allowing light to reflect back and forth, thereby amplifying the laser output. The partially reflective mirror permits a portion of the light to escape as the laser beam. And a cooling system is generally necessary due to the considerable heat produced during operation.

The Nd: YAG laser functions as a four-level laser system:

Excitation: When the flash lamp or diode is powered on, it produces light that excites Nd^{3+} ions from their ground state to higher energy levels.

Non-radiative Relaxation: Excited ions rapidly transfer to a metastable energy level (E_3) through non-radiative processes.

Population Inversion: The metastable state has a relatively extended lifetime, facilitating the creation of a population inversion between E_3 and a lower energy level (E_2).

Stimulated Emission: Once population inversion is established, stimulated emission occurs as ions transition from E_3 to E_2, emitting photons at a wavelength of 1.064 µm. These photons are amplified within the optical cavity, and a portion escapes through the output coupler as the laser beam.

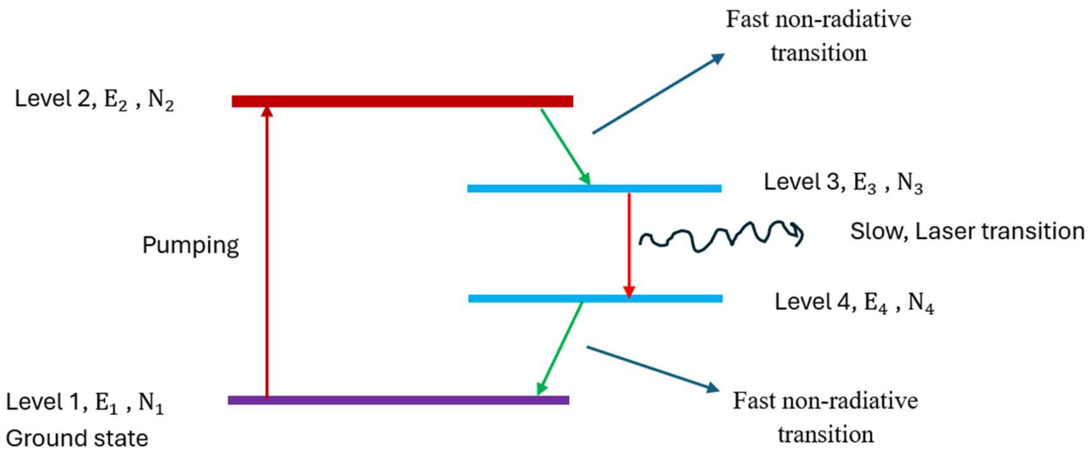

Fig. 1.9: Schematic diagram of four level energy laser.

Because it can function in both continuous wave (CW) and pulsed modes, the Nd: YAG laser is extremely adaptable for use in scientific (i.e. Spectroscopy, nonlinear optics, and as a pump source for other lasers), industrial (i.e. Cutting, welding, drilling, and marking of metals and non-metals, especially for precision tasks and reflective materials), medical (Dentistry, dermatology, ophthalmology such as laser eye surgery, and other surgical specialties because of its accuracy and capacity to reduce tissue damage) and military (Range assessment, target identification, and lidar technologies) .

1.1.2.3.2 **Introduction to semiconductor laser**: Semiconductor lasers, often referred to as laser diodes, are solid-state devices that produce coherent light through stimulated emission within a semiconductor gain medium, typically a forward-biased PN junction made from direct bandgap materials such as gallium arsenide (GaAs) [1]. When electrically energized, electrons and holes come together at the junction, releasing photons whose energy aligns with the bandgap of the material. For lasing to occur, the active medium is enclosed between p-type and n-type cladding layers, creating a double heterostructure that confines both carriers and light within the junction [6]. The ends of the structure are polished to form an optical resonator, allowing for light amplification through continuous reflection and stimulated emission. These lasers are known for their high efficiency, compact design, and capacity for rapid output modulation, making them well-suited for Fiber-optic communication, barcode scanners, and optical data storage [6]. They emit light across a spectrum that ranges from visible to infrared wavelengths, with uses in laser cutting, welding, medical imaging (like optical coherence tomography), and photodynamic therapy. Additionally, semiconductor lasers are fundamental to innovative technologies such as optical tweezers for cell manipulation and high-power direct diode systems for processing industrial materials. Their low power consumption and reliability have secured their position as essential components in contemporary optoelectronics and telecommunications.

1.1.2.3.3 **Introduction to Nd: Glass laser:** Nd: Glass lasers are solid-state lasers that use neodymium-doped silicate or phosphate glass as the active medium, producing near-infrared wavelengths of 1.062 μm (for silicate) or 1.054 μm (for phosphate) through the process of stimulated emission [6]. The laser function based on a four-level energy scheme: optical pumping elevates Nd^{3+} ions to an upper energy level 2, which then undergoes nonradiative decay to a metastable state at level 3. A population inversion between levels 3 and 4 allows for the laser transition, with spontaneous emission bringing ions back to the ground state at level 1. The gain medium is contained within a resonator cavity equipped with highly reflective and partially reflective mirrors to enhance light amplification.

The key benefits include a uniform doping distribution, isotropic properties, and versatility in forming the glass into various shapes such as rods, disks, or Fibers. However, their thermal conductivity is lower compared to crystal-based lasers (like Nd: YAG), limiting their continuous-wave operation and making them more suitable for high-energy pulsed applications, such as laser welding and drilling. Their broad emission linewidth raises the thresholds for amplification but permits tunability when paired with diffraction gratings.

1.1.2.3.4 **Introduction to Fiber laser:** A Fiber laser is a kind of solid-state laser that uses an optical Fiber as its active gain medium, which is infused with rare-earth elements such as ytterbium, erbium, or neodymium. The laser process initiates with pump light generated by laser diodes, which is directed into the core of the Fiber—a pathway made of silica glass that is coated with the selected rare-earth dopant. The cladding surrounding the core has a lower refractive index, which helps to keep the light contained within the core through total internal reflection, enabling effective energy transfer and amplification. As the pump light moves through the doped area (the laser cavity), stimulated emission takes place, leading to the generation of a highly collimated and coherent laser beam at a specific wavelength defined by the dopant. Fiber lasers are celebrated for their high efficiency in converting electrical power to optical power, outstanding beam quality, and compact, durable construction. Their elongated, slender design offers a large surface area for efficient heat dissipation, facilitating continuous high-power operation with minimal thermal distortion. These characteristics make Fiber lasers particularly suitable for industrial uses such as cutting, welding, engraving, and marking metals, as well as for applications in telecommunications, medical procedures, and scientific research. Moreover, Fiber lasers are known for their reliability, long operational life, and low maintenance demands, although they may involve higher upfront costs and may not be as effective for cutting certain non-metal materials compared to alternatives like CO_2 lasers.

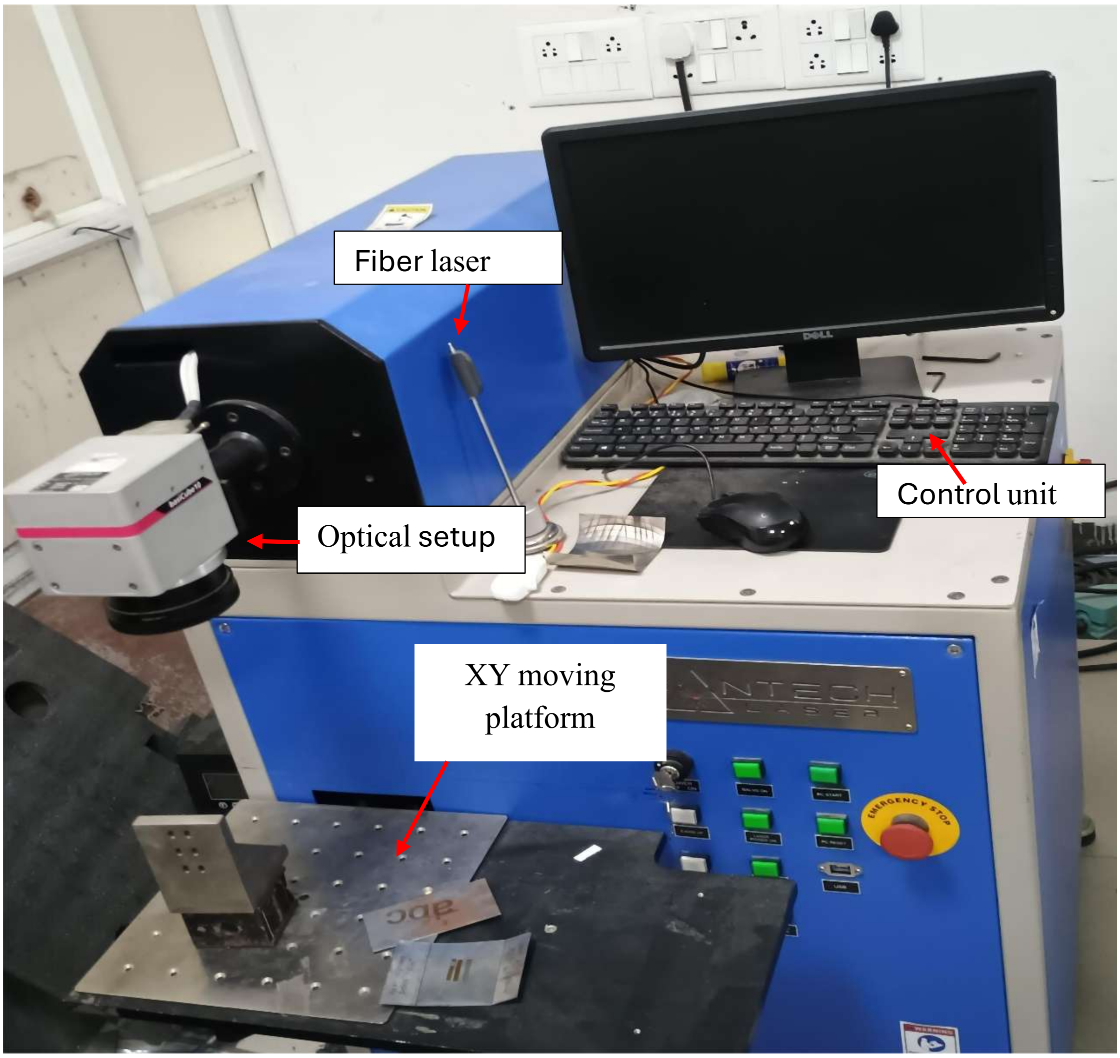

Fig. 1.10: Image of Fiber laser setup at IITI.

1.1.3 **Laser safety and hazardous:** Laser safety refers to the procedures and safety measures used to reduce the possibility of laser radiation harm, especially to the skin and eyes, as well as non-beam risks associated with laser systems [1]. Because of their powerful, concentrated light beams, lasers can inflict significant harm; therefore, their usage must be carefully controlled and protected. The risk of serious skin and eye damage from direct and reflected laser beams, as well as related non-beam risks including electrical shock and fire, makes laser safety crucial [1]. Effective laser hazard control requires knowledge of laser classes, adherence to maximum allowable exposure limits, use of suitable protective gear, and adherence to safety guidelines and training [1].

1.2 **Introduction to laser cutting:** The idea of utilizing light to slice materials has fascinated individuals ever since they discovered they could ignite paper using a magnifying glass and sunlight. The capability to cleave through thick steel with a laser is even more remarkable. Currently, laser cutting stands as the most prevalent industrial application of lasers. In Japan, for instance, around 80% of industrial lasers are allocated to this function [1]. Although the allure of technology is certainly captivating, it isn't the primary reason that industries invest in it. The main advantage is that laser cutting can effectively substitute conventional cutting methods in current markets—and it frequently does so with enhanced speed and accuracy compared to other approaches [1]. So, due to its obvious and useful benefits over conventional cutting techniques—speed, accuracy, flexibility, and cost-effectiveness—laser cutting has evolved from an intriguing concept to a widely used industrial tool.

1.2.1 **The process of laser cutting:** Laser cutting is recognized as one of the fastest material cutting techniques. It operates without physical contact between a tool and the workpiece, which eliminates tool wear and extends equipment life. Though clamping the workpiece is not strictly necessary, it is often recommended to prevent unwanted movement due to table acceleration, especially when using CNC programs. The process is highly flexible, as tool changes are software-based rather than mechanical, allowing for easy and rapid alterations in cutting patterns [1].

Laser cutting is quiet and well-suited for automation, with future potential for adaptive control systems. The beam can cut in any direction depending on polarization, and it handles a wide range of materials—including brittle, soft, hard, conductive, and non-conductive substances. However, highly reflective materials like aluminium, copper, and gold may present challenges, though these can be overcome with precise beam control.

The system includes the laser source, shutter mechanism (typically a retractable mirror that blocks or allows beam passage), beam guidance optics, focusing components, and a motion system to direct either the beam or the workpiece. The focusing optics can be transmissive (using materials like ZnSe, GaAs, or quartz) or reflective (using shaped mirrors), depending on laser type and thermal requirements.

After focusing, the laser beam passes through a nozzle with a coaxial gas jet, which helps in material removal and protects optics from debris. In setups using metal optics—preferred for high-power lasers or educational environments prone to damage—an "air knife" may be used to deflect smoke and spatter. Specialized nozzle designs, like centrally directed or ring jets, ensure effective gas flow without compromising the metal optics.

Proper alignment of the laser beam, optics, and gas jet is critical for optimal cutting. The process starts by drilling or piercing a hole, especially when the cut doesn't begin at an edge. Piercing differs from linear cutting because it creates a closed hole rather than an open-ended path. This drilling step is essential to initiate the cutting process.

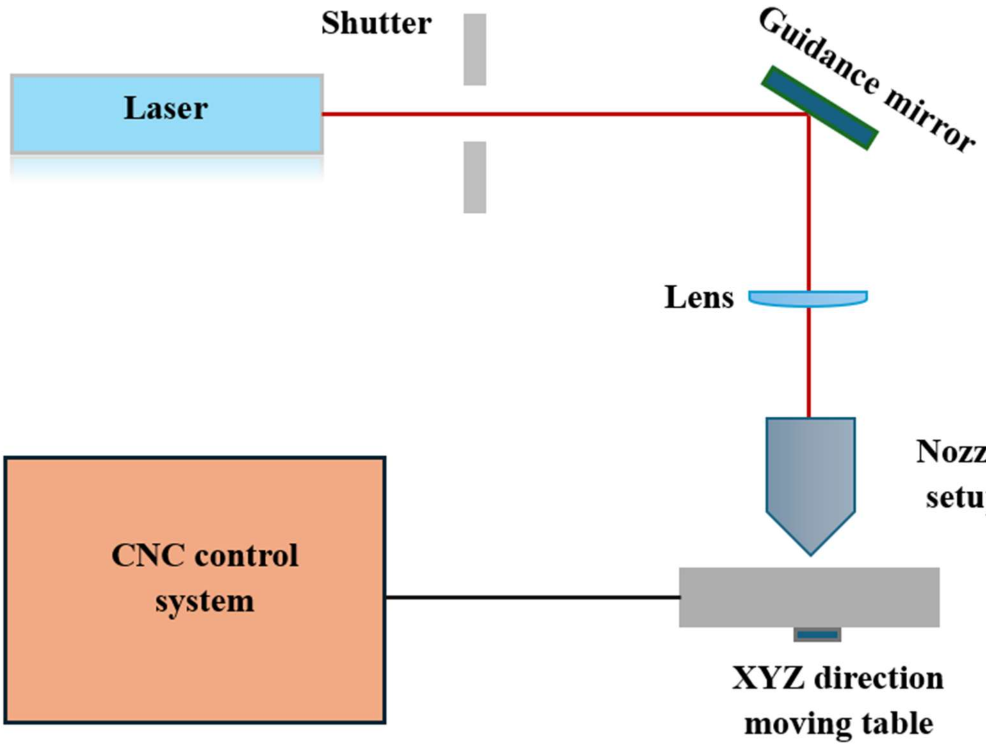

Fig. 1.11: Schematic diagram of laser cutting/drilling setup.

1.3 **Introduction to laser drilling:** Laser drilling is a precise, non-contact method that creates openings in a variety of materials by concentrating intense laser light on a workpiece, where the energy transforms into heat, resulting in localized melting and vaporization (ablation) of the material. In contrast to conventional drilling, which utilizes a rotating physical bit, laser drilling utilizes pulsed laser beams—ranging from femtosecond to millisecond durations—to remove material in controlled steps, enabling the fabrication of holes with diameters as small as a few microns and high aspect ratios (depth-to-diameter), sometimes surpassing 10:1. This technique offers high flexibility, allowing for the drilling of holes at different angles, depths, and shapes, and is effective on metals, ceramics, glasses, polymers, and even challenging materials like diamonds. As a non-contact technique, laser drilling eliminates tool wear and reduces mechanical stress on the workpiece, producing smooth, precise holes with minimal heat-affected zones and no swarf generation. Laser drilling is extensively applied in sectors such as aerospace, automotive, electronics, and medical device manufacturing, where high precision and consistency are essential [1].

1.3.1 **Advantage of laser drilling**: It provides some control over burrs and splatter and can drill holes quickly. No matter how hard the material is, it can bore through it if it can absorb the radiation. The hole may puncture materials at almost any angle and its diameter and form can be accurately adjusted with trepanning processes. Increasing drilling speed, minimizing or controlling hole taper, preventing spatter, reducing or eliminating the resolidified layer on the hole walls, producing high-aspect-ratio holes, producing precise hole shapes (whether round, square, or star-shaped) to ensure consistency and repeatability, and efficiently drilling through coated materials are some of the current processing challenges being addressed.

1.3.2 **Types of laser drilling:** There are various types of laser drilling, and each is appropriate for a particular application and hole size. single pulse drilling, Trepanning, percussion drilling, and helical trepanning are the main types [1]. In contrast to single pulse drilling, percussion and trepanning offer superior control and finer outcomes. These types vary in speed, accuracy, and hole quality. For some materials and hole geometries where continuous spiral motion is beneficial, helical drilling offers an option.

1.3.2.1 **Single pulse drilling:** Single pulse laser drilling is a precise method for removing material, where a high-energy, quick laser pulse is aimed at a specific spot on a workpiece to create a hole in a single attempt. The energy from the laser pulse is absorbed by the material's surface, resulting in rapid localized heating, melting, and frequently vaporization. This extreme thermal interaction creates a high-pressure vapor plume that aids in expelling molten material from the hole, resulting in a clean and typically narrow hole with a limited heat-affected zone

(HAZ). As the process is completed in just one pulse, it is especially beneficial for creating micro-holes in tough or brittle substances like ceramics, metals, or composites, particularly in sectors that demand high precision and speed, such as aerospace, electronics, or the manufacturing of medical devices. The quality of the hole produced is influenced by various factors, including pulse duration, energy, wavelength, and focal spot size, all of which are meticulously optimized to achieve the intended hole shape while reducing thermal damage or recast layers. The size of the resulting hole is closely linked to the focus spot size of the laser and the energy provided in each pulse. In general, single pulse drilling is appreciated for its straightforwardness, speed, and its effectiveness in situations where rapid production is more important than achieving the highest quality of holes [1, 7].

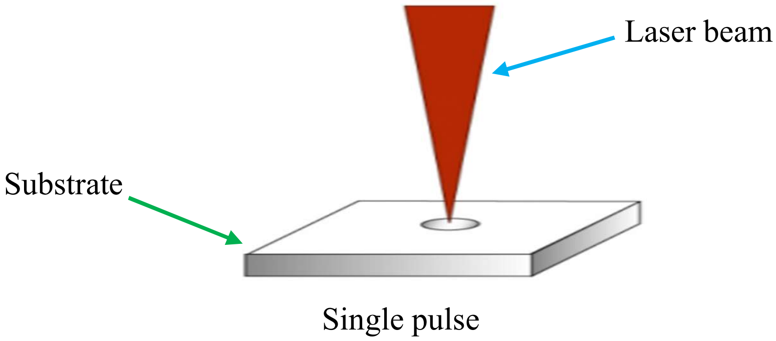

Fig. 1.12: Schematic diagram of single pulse laser drilling.

1.3.2.2 **Percussion drilling:** Laser percussion drilling is a method that involves directing a sequence of laser pulses at a stationary point on a material to create a hole by gradually removing small bits of material with every pulse [7]. In contrast to single-pulse laser drilling, which utilizes one powerful burst to form a hole, percussion drilling makes use of multiple, lower-energy pulses, which facilitates the creation of deeper and more accurate holes, generally with smaller diameters and higher aspect ratios (depth-to-diameter ratios). Throughout the process, the concentrated laser energy is absorbed by the material, leading to rapid heating, melting, and occasionally vaporization (ablation) of the targeted area. The vapor and molten material produced are expelled from the hole, often assisted by a processing gas to enhance efficiency and improve the quality of the hole. In percussion drilling, there is no movement between the laser beam and the workpiece, setting it apart from other techniques such as trepanning, where the laser moves in a pattern around the edge of the desired hole. This method is especially well-suited for creating small-diameter, high-quality holes in various materials, including metals, ceramics, and composites, and is commonly employed in applications such as cooling holes for aerospace turbines and micro-vias in printed circuit boards. The efficiency of the process and the quality of the holes achieved are influenced by factors such as pulse duration, energy, frequency of repetition, and the characteristics of the workpiece material [7].

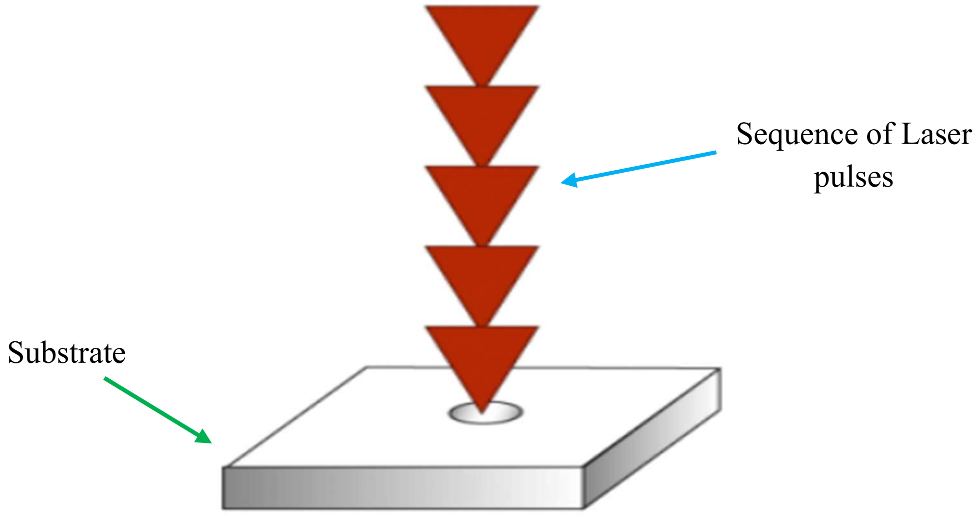

Fig. 1.13: Schematic diagram of laser percussion drilling.

1.3.2.3 **Trepanning:** Laser trepanning is a precise machining method designed to form holes in different materials using a laser beam that moves along a defined circular path [8]. This can involve either the movement of the laser spot itself or the rotation of the workpiece, such that the outer boundary of the laser spot touches the specified hole diameter. In contrast to percussion drilling, which works by delivering repeated pulses to a single location, trepanning only removes material from a narrow annular area around the intended hole's edge. This makes trepanning more energy-efficient and results in a reduced heat-affected zone (HAZ) along with better hole quality. There are primarily two methods: mechanical trepanning, where the laser or the workpiece is physically manipulated, and optical trepanning, which utilizes specialized optics to shape the laser beam into a ring-like profile that remains still while removing material. Optical trepanning is beneficial as it removes the need for moving parts, enhances system dependability, and can considerably cut down processing times using beam-splitting techniques to drill multiple holes simultaneously. The parameters of the process, including laser pulse duration, energy output, and scanning speed, are meticulously adjusted to manage the hole diameter, tapering, and surface finish. Laser trepanning is particularly well-suited for creating high-quality, precise holes with minimal taper and recast layer, making it a common choice in industries that require micro-holes or complex hole shapes in metals, ceramics, and other difficult-to-machine materials [9].

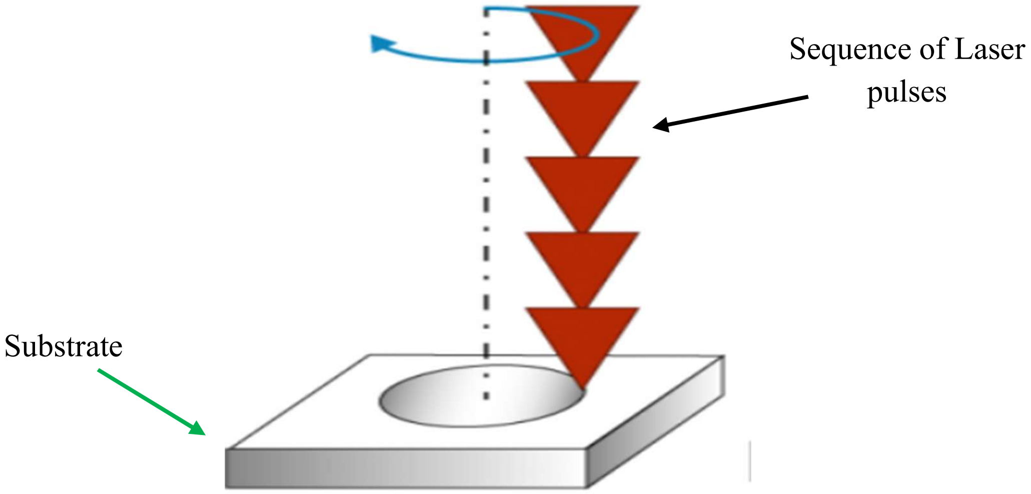

Fig. 1.14: Schematic diagram of trepanning.

1.3.2.4 **Helical trepanning:** Laser helical trepanning is a sophisticated laser drilling method in which the laser beam, along with its focus, is maneuvered in a controlled helical (spiral) trajectory to create openings in a material. [7] Unlike conventional trepanning, which involves cutting out the shape of a hole by rotating the beam in a circular motion, helical trepanning directs the laser focus along a three-dimensional helical route—merging both circular and axial (depth-wise) movements. This technique enables the laser to progressively ablate the material layer by layer, yielding holes with high aspect ratios and enhanced surface quality. The helical trajectory can be customized to create either cylindrical or conical openings, based on the desired shape. A significant benefit of this technique is that it reduces or completely eliminates recast layers and thermal damage, which are frequent issues in percussion drilling, resulting in cleaner and more accurate holes. Helical trepanning is especially efficient for creating deep, large-diameter holes, as the majority of the molten material is effectively expelled upward out of the hole during the process. Furthermore, this method can be improved with optimized laser settings and the incorporation of process gases, making it an excellent choice for applications that demand high precision and superior hole quality, such as in micromachining and advanced manufacturing.

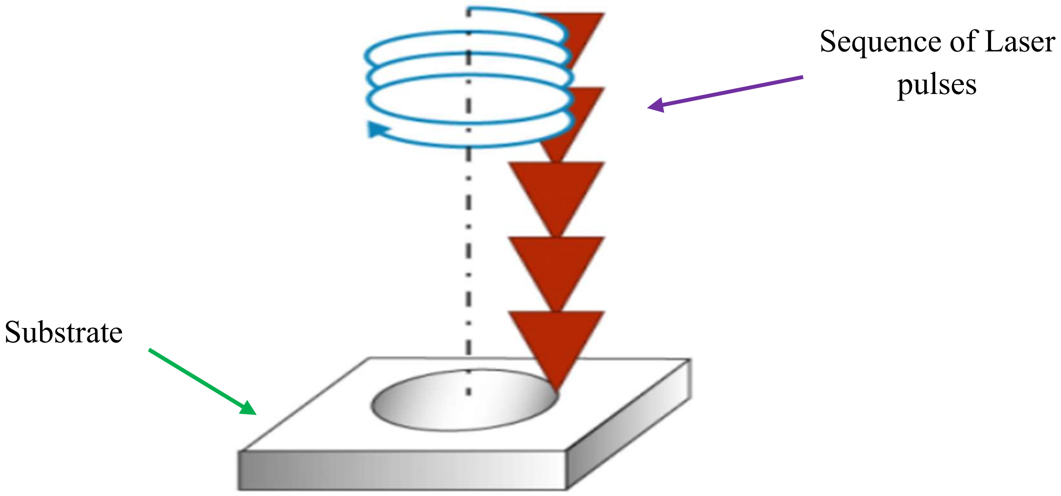

Fig. 1.15: Schematic diagram of helical trepanning.

1.4 **Overview of workpiece material SS316:** Stainless steel 316 (SS316) is an exceptionally adaptable and commonly utilized austenitic stainless-steel alloy, recognized for its superior corrosion resistance in comparison to standard grades like SS304. This enhancement is chiefly attributed to the intentional inclusion of 2–3% molybdenum along with 16–18% chromium and 10–14% nickel. Such a composition significantly increases its resistance to both pitting and crevice corrosion, particularly in environments rich in chlorides and acids, establishing SS316 as the preferred material for uses in marine, chemical processing, pharmaceutical, and food sectors. The alloy demonstrates outstanding mechanical properties, featuring a minimum tensile strength of 579 MPa, good ductility (with an elongation of 50%), and toughness even at cryogenic temperatures. SS316 is non-magnetic in its annealed state, although it may develop slight magnetism when subjected to cold working. It is also highly suitable for various fabrication methods, including welding, forming, and machining, albeit it cannot be hardened through heat treatment and is generally annealed at approximately 1900°F (1040°C) to alleviate internal stresses. The low-carbon variant, SS316L, is favored for welded structures due to its resistance to sensitization and intergranular corrosion. The ability of SS316 to withstand a wide array of chemicals, such as sulfuric, hydrochloric, acetic, and tartaric acids, further enhances its utility in industrial settings, while its durability, formability, and resistance to temperature extremes solidify its role as a key material in challenging conditions. Thus, SS316 is selected due to its combination of resistance to corrosion, longevity, cleanliness, and environmental sustainability, which makes it a dependable and effective material for challenging conditions.

Chapter 2

Literature Survey, Objectives and Methodology

The process of laser drilling stainless steel SS316 involves a complex thermal mechanism, where the settings of the laser play a crucial role in determining quality factors such as the quality of the holes, the roughness of the surface, and the heat-affected zone (HAZ) [10]. Both theoretical modelling and experimental validation have been thoroughly researched to refine these parameters for enhanced drilling efficiency.

Theoretical models for laser drilling often employ computational approaches like finite element methods (FEM) and mathematical formulations that assume axisymmetric conditions to simulate the distribution of temperature, material removal, and phase transitions throughout the drilling process [11]. These models take into account factors such as laser focus, pulse duration, laser energy, and energy absorption dynamics in order to forecast drilling performance and fine-tune parameters [12]. Additionally, the models examine rates of melt ejection and vaporization, which affect the speed of drilling, and the quality of the holes produced. Thermal modelling is essential for understanding heat transfer and the resulting melting and vaporization of materials, both of which are vital for achieving high machining quality.

Experimental studies involve the deliberate alteration of laser parameters such as pulse width, energy, pulse frequency, and assist gas pressure to assess their impact on drilling quality traits including heat-affected zone (HAZ), surface roughness, hole diameter, taper, and circularity [13]. Nd: YAG and CO2 lasers are often utilized because of their effectiveness in machining SS316, with experiments utilizing Taguchi designs and Grey Relational Analysis (GRA) for multi-objective optimization [14]. Research indicates that higher laser power and pulse frequency typically lead to an increase in HAZ and surface roughness because of greater thermal load [14]. The use of assist gas pressure aids in minimizing the molten material around the hole, thus reducing HAZ. Confirmation through microscopy and surface morphology examinations validates the impact of parameters on hole quality [14].

Methods for multi-criteria optimization, such as Taguchi's method paired with Grey Relational Analysis, are commonly used to enhance laser drilling parameters to minimize both heat-affected zone (HAZ) and surface roughness at the same time [14]. These approaches aid in determining the best combinations of factors such as gas pressure, laser power, and pulse frequency values that enhance product quality while lowering machining expenses [14].

Analysis comparing laser drilling with traditional drilling reveals that laser drilling presents benefits like non-contact machining, enhanced precision, and greater reproducibility [15]. Research conducted on different stainless-steel grades (like AISI 304) and alloys (including nickel-based superalloys and titanium alloys) offers valuable insights into how laser parameters and auxiliary gases impact performance traits, which can guide SS316 drilling methods.

Low et.al., [16]. The paper discusses the development of a one-dimensional mathematical model for gas-assisted low power laser metal drilling, focusing on the gas-assisted molten metal expulsion concept. It builds upon an existing analytical hydrodynamic model to incorporate the effects of using O2 assist gas, analysing its impact on melt surface temperature, ejection velocity, and drilling velocity. The study emphasizes the importance of numerical methods and programming in validating the model under practical drilling conditions.

Ng, G. K. L., et.al., [17]. The literature on laser drilling encompasses various analytical and numerical models that evaluate the effects of laser parameters on temperature profiles, removal rates, and hole geometries. Key contributions include the integral models by Semak and Matsunawa, which incorporate mass and energy conservation principles, and the adaptation of these models to include assist gases. Recent advancements focus on higher-dimensional numerical models, reflecting the growing computational capabilities and the need for more accurate simulations in laser materials processing.

Kaplan, A. F., et.al., [18]. The article presents an analytical model for laser beam cutting of metals, focusing on the physical state at the cutting front rather than the quality of the cutting edges. It incorporates various simplifying assumptions to maintain practicality while being sufficiently realistic, utilizing mass, momentum, and energy balances. Recent advancements in understanding gas flow behaviour and melt flow phenomena are also discussed, highlighting the importance of these factors in the laser cutting process.

Ghoreishi et.al., [19]. The study investigates the effects of six controllable variables on hole taper and circularity in laser percussion drilling of stainless steel and mild steel. A central composite design (CCD) and response surface methodology (RSM) were employed to efficiently analyse the interactions between variables such as laser peak power, pulse width, and assist gas pressure. The results indicate that while certain parameters significantly affect hole characteristics, the traditional one-factor-at-a-time approach is less effective compared to the designed experiments that can reveal interactions and optimize outcomes.

Dubey, A. K., et.al., [20]. This study employs the Taguchi methodology to optimize the laser beam cutting process of aluminum alloy sheets, a challenging material due to its reflective and thermal properties. The research aims to identify optimal controllable parameters, including oxygen pressure, pulse width, pulse frequency, and cutting speed, to enhance key performance characteristics such as taper angles and material removal rate (MRR). The methodology involves selecting appropriate orthogonal arrays, calculating signal-to-noise ratios, and performing analysis of variance (ANOVA) to determine the significance of each factor. The results demonstrate a considerable improvement in both taper angle and MRR through an integrated robust design approach. Moreover, the study advances to multi-objective optimization using the Taguchi quality loss function, concurrently improving multiple quality characteristics. The findings reveal that multi-objective optimization causes only a slight increase in taper angle compared to single-objective optimization while maintaining the same MRR, indicating its effectiveness in achieving a balanced enhancement of process performance. Overall, the research provides valuable insights into process parameter optimization for laser cutting of difficult-to-machine reflective metals, emphasizing the importance of multi-objective approaches for comprehensive quality improvement.

2.1 Objectives of the study:

1. **Experimental Investigation for Quality Metrics:** To experimentally investigate and evaluate the quality of laser-drilled holes with a focus on maximizing circularity, minimizing taper angle, and determining the depth of cut per laser pulse under varying process parameters.

2. **Optimization of the Laser Drilling Process:** To optimize the laser drilling parameters to achieve improved hole quality and machining efficiency, using statistical methods, or optimization algorithms.

3. **Analysis of Laser Process Parameters:** To analyse the influence of key laser parameters such as pulse energy, pulse duration, frequency, and focal position on the output characteristics of the laser drilling process including hole geometry and material removal rate.

4. **Theoretical Modelling of Depth of Cut:** To develop a theoretical model that predicts the depth of cut achieved in single-pulse laser drilling operations for different laser energy inputs, providing a mathematical understanding of material removal mechanisms.

5. **Experimental Validation of the Theoretical Model:** To validate the accuracy of the developed theoretical model through comparison with experimental results, ensuring the model's reliability in predicting depth of cut and process behavior.

6. **Comparison Between Theoretical and Experimental Results:** To perform a critical comparison between the outcomes of theoretical predictions and experimental observations, assessing deviations and identifying potential areas for model improvement or process refinement.

2.2 Problem statement

Laser drilling is widely utilized in industries requiring precision micro-machining, particularly for difficult-to-machine materials like austenitic stainless steels (e.g., SS316). Despite its advantages in terms of non-contact material removal and high aspect ratio hole formation, achieving high-quality holes with minimal taper, maximum circularity, and consistent depth remains a significant challenge. Variability in laser parameters such as pulse energy, duration, and focus leads to inconsistent hole geometry, reduced dimensional accuracy, and suboptimal machining performance. While several empirical studies have addressed parameter optimization, there is a lack of robust theoretical frameworks that can accurately predict the depth of cut and material removal behavior under varying laser energy conditions. Furthermore, the complex interaction of thermal and fluid dynamics during laser-material interaction remains inadequately understood and modeled, particularly for single-pulse drilling scenarios. There is a critical need for a comprehensive approach that combines experimental investigation, statistical optimization, and theoretical modeling to enhance the understanding and control of the laser drilling process. Developing a validated theoretical model that captures the physics of laser-material interaction and aligns with experimental observations would provide a powerful tool for predicting and optimizing drilling outcomes.

This research aims to address this gap by experimentally investigating the laser drilling process of SS316, optimizing the process parameters using the Taguchi method, developing a hydrodynamic theoretical model for single-pulse drilling, and validating this model through experimental comparison to ensure both predictive accuracy and practical applicability.

2.3 Methodology of the study:

1. **Material Selection and Preparation:** Stainless steel grade SS316 was chosen for the laser drilling experiments because of its common industrial use and difficult machining characteristics. The workpieces were manufactured to specific dimensions to maintain uniformity in the experimental trials. Before undergoing laser processing, the surfaces were cleaned to eliminate impurities and oxidation.

2. **Laser Drilling Experiments:** Laser drilling was conducted utilizing a pulsed laser system, with the ability to control essential process variables like laser energy, pulse duration, pulse frequency, and focal position. A variety of holes were created with different combinations of parameters to analyse the resulting geometric characteristics. Important response parameters—including hole circularity, taper angle, and cut depth—were assessed using optical microscopy and image processing methods. The depth of penetration was additionally confirmed through cross-sectional metallography.

3. **Design of Experiments and Optimization using Taguchi Method:** To systematically analyse how laser parameters affect output responses and to find the best processing conditions, the Taguchi method was utilized. An L16 orthogonal array was chosen to reduce the number of required experiments while enhancing the amount of information gathered. Signal-to-noise (S/N) ratios were computed for each output parameter based on the optimization objectives: “Larger-the-better” for hole circularity, “Smaller-the-better” for taper angle, and “Larger-the-better” for depth of cut.

4. **Theoretical Modelling of Laser Drilling using Hydrodynamic Approach:** A theoretical model based on physics was created to estimate the depth of cut generated by a single laser pulse. This model utilizes principles of energy balance and considers the thermal and hydrodynamic behaviour that occurs during the interaction between the laser and the material. The primary assumptions include: the immediate absorption of laser energy at the surface of the material, the main mechanism for material removal being vaporization, and insignificant

thermal conduction losses during the duration of a single pulse. By solving conservation equations for mass, momentum, and energy in the molten zone, the model computes the rate of melt ejection and material removal driven by vaporization, considering the distribution of laser intensity and the fluid dynamics of the molten flow.

5**. Experimental Validation of Theoretical Model:** The predictions made by the theoretical model regarding the depth of cut per individual pulse at different laser energy levels were compared to values obtained from experiments. The differences were examined, and the model was refined through several iterations to address experimental uncertainties like variations in the heat-affected zone and losses in laser energy.

6. **Comparative Analysis:** A detailed comparison was made between the experimental findings and theoretical predictions. The precision of the theoretical model was measured using percentage error, and its reliability was examined across different energy levels and operational conditions. This comparative analysis reinforced confidence in the proposed model and offered insights into the constraints and assumptions that exist within the theoretical framework.

Chapter 3

Experimental Investigations

3.1 **Laser material interaction:** When laser light strikes a material, the interaction process initiates with the division of the incoming energy into two main components: absorption and reflection. A fraction of the laser light is absorbed by the material, which depends on its optical properties, including the absorption coefficient and surface characteristics. This absorbed energy can cause various physical and chemical alterations within the material, such as heating, melting, vaporization, or even ionization, depending on factors like laser intensity and pulse duration. At the same time, another fraction of the laser light is reflected from the surface, with the quantity of reflection influenced by factors such as the surface finish, angle of incidence, and refractive index mismatch between the material and its environment. The ratio of absorbed to reflected energy determines the effectiveness and characteristics of the laser-material interaction, which is crucial for applications like laser cutting, welding, engraving, and surface modification.

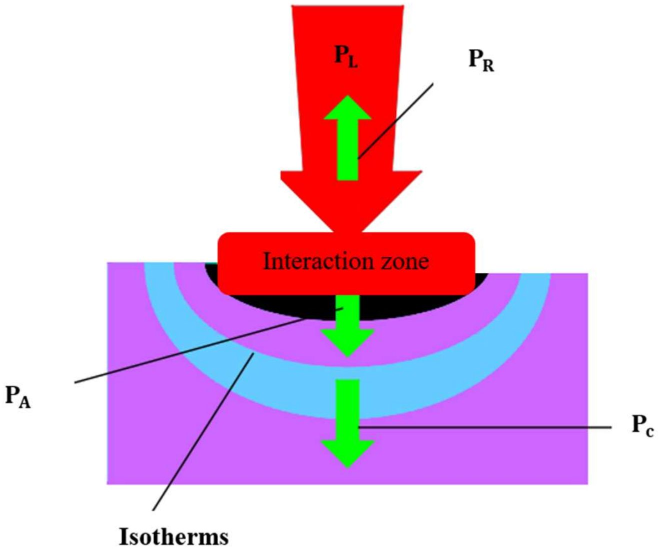

Fig. 3.1: Laser material interaction diagram.

- $\mathbf{P_L = P_A + P_R = AP_L + RP_L}$

Where, P_L = Incident laser power, P_R = Reflected laser power, A= Coefficient of absorption, R = Coefficient of reflectivity

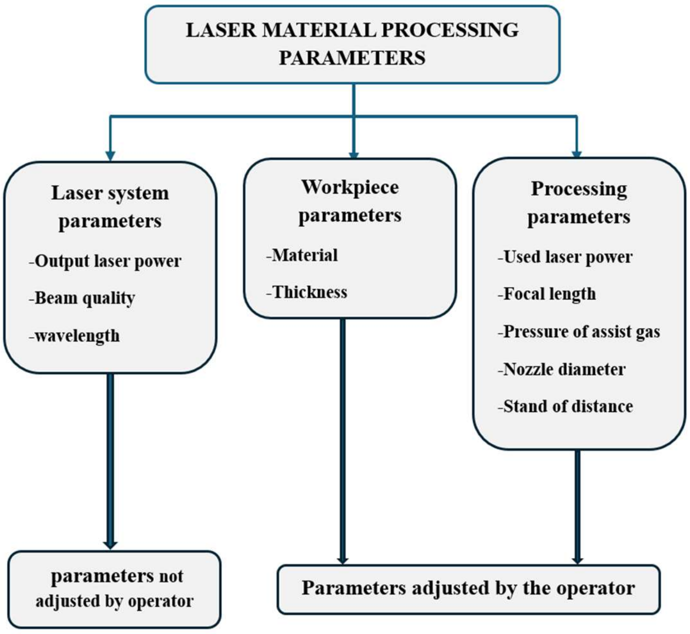
LASER MATERIAL PROCESSING PARAMETERS
Laser system parameters
-Output laser power
-Beam quality
-wavelength
Workpiece parameters
-Material
-Thickness
Processing parameters
-Used laser power
-Focal length
-Pressure of assist gas
-Nozzle diameter
-Stand of distance
parameters not adjusted by operator
Parameters adjusted by the operator

Fig. 3.2: Laser material processing parameters.

Intensity level required for different phenomena: The intensity level requirements for various laser-based processes vary depending on the desired application. For heating processes such as heat treatment and hardening, an intensity of approximately 10^4 to 10^5 W/cm² is required. Melting applications including soldering, spot welding, marking, melt cutting, and surface treatment demand higher intensities in the range of 10^5 to 10^7 W/cm². Vaporization processes like drilling, sublimation cutting, scribing, trimming, penetration welding, and shock hardening require even greater intensities, ranging from 10^7 to 10^8 W/cm². Plasma shielding effects occur at intensities between 10^8 and 10^{10} W/cm², while gas breakdown phenomena are observed at extremely high intensities, typically between 10^{10} and 10^{12} W/cm².

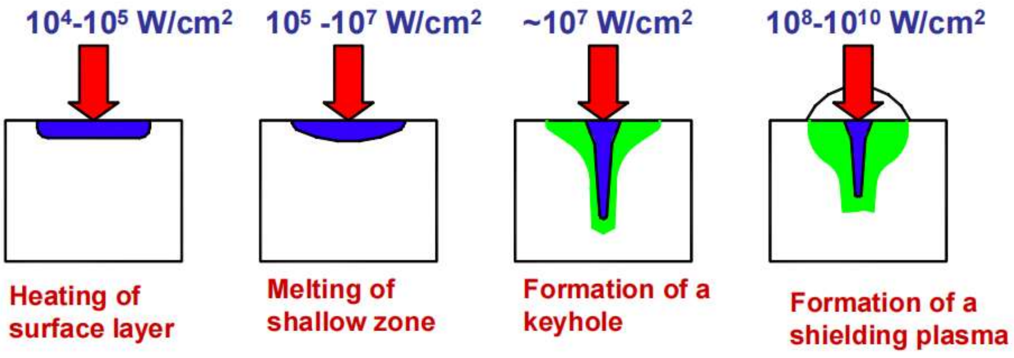
10^4-10^5 W/cm^2
10^5 -10^7 W/cm^2
~10^7 W/cm^2
10^8-10^{10} W/cm^2
Heating of surface layer
Melting of shallow zone
Formation of a keyhole
Formation of a shielding plasma

Fig. 3.3: Level of intensity required for different phenomena.

3.2 **Experimental setup:** In the experimental setup, a fiber-coupled pulsed Nd: YAG laser with a wavelength of 1.064 µm, peak power 5kW and average power 250 W is employed as the primary laser source. The use of an optical fiber allows for flexible and efficient transmission of the laser beam, making it particularly suitable for operations in remote or hard-to-access areas. The laser beam is directed through a specially designed optical setup integrated with a nozzle, which aids in precise beam focusing and assists in material interaction. Additionally, the system is mounted on a computer numerical control (CNC) machine, enabling controlled and programmable movement of the laser head. This integration ensures high precision and repeatability in the processing tasks, making the setup ideal for a range of laser-based material processing applications.

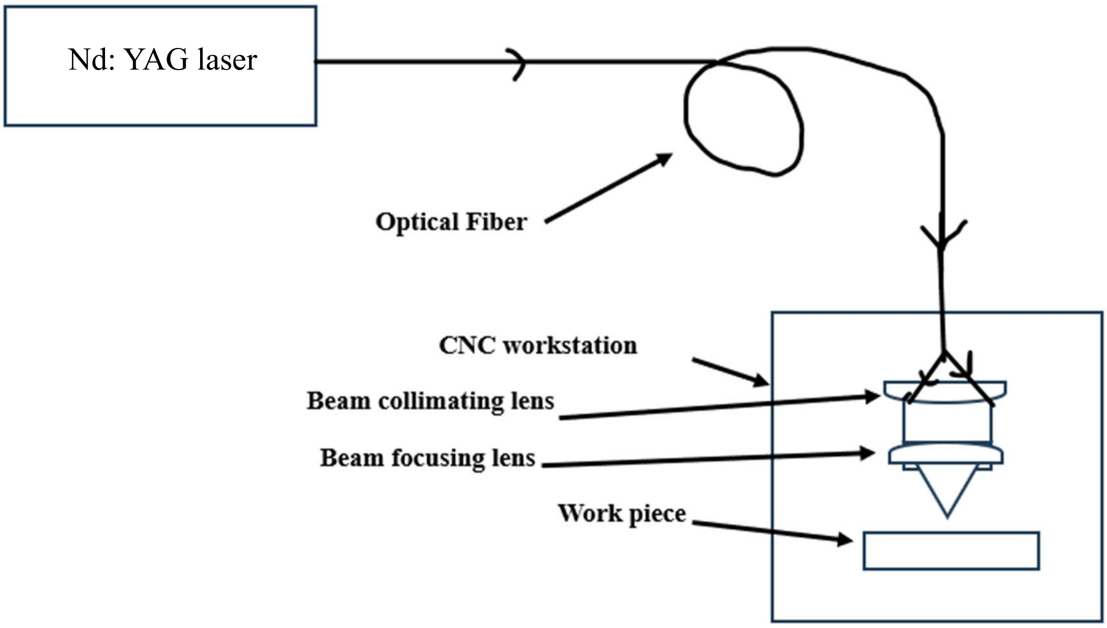
Nd: YAG laser
Optical Fiber
CNC workstation
Beam collimating lens
Beam focusing lens
Work piece

Fig. 3.4: Schematic diagram of laser drilling setup.

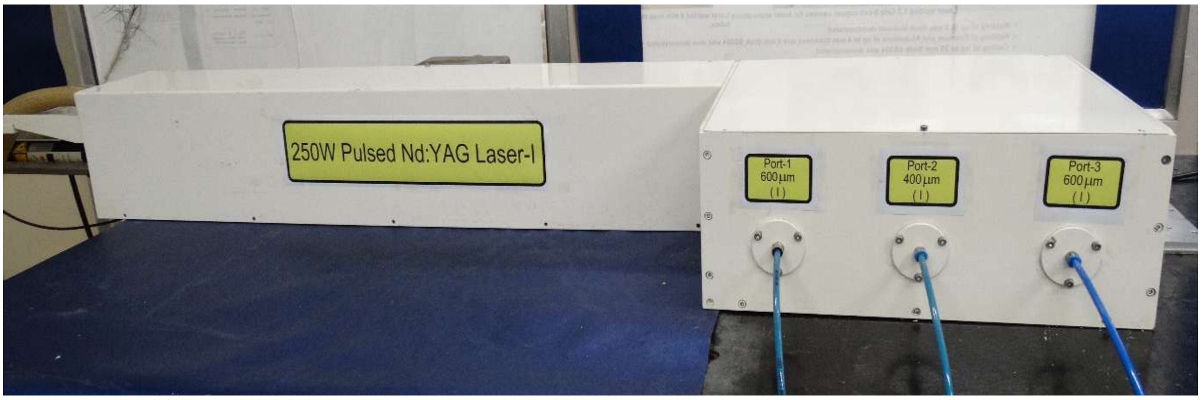
250W Pulsed Nd:YAG Laser-I
Port-1
600µm
(I)
Port-2
400µm
(I)
Port-3
600µm
(I)

Fig. 3.5: 250 W average power and 5kW peak power industrial Nd: YAG laser with multi-port fiber optic beam delivery at RRCAT, Indore.

3.3 **Experimental details:** The experimental work was conducted on 3 mm thick stainless steel (SS316) specimens using a Fiber-coupled pulsed Nd:YAG laser as the source. The laser system is capable of delivering a peak power of 5 kW with an average output power of 250 W. The laser beam, transmitted through an optical fiber, is focused to a spot diameter of approximately 400 µm. A standoff distance of 1.5 mm between the nozzle and the workpiece was maintained during the experiments to ensure optimal beam focus and interaction with the material. Compressed air was used as the assist gas to facilitate the removal of molten material and to maintain the quality of the processed surface. These parameters were carefully selected to achieve efficient and controlled laser processing of the stainless-steel samples.

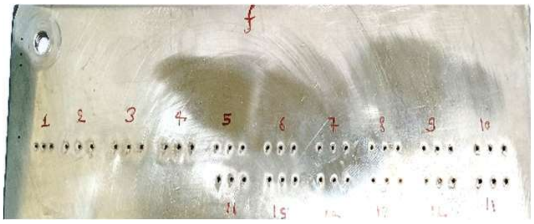

Fig. 3.6: Image of laser drilled sample top side.

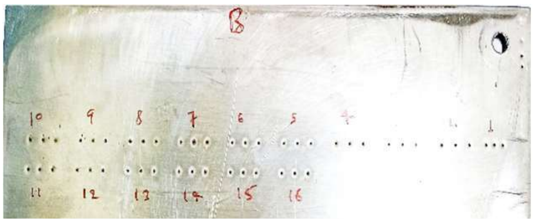

Fig. 3.7: Image of laser drilled sample bottom side.

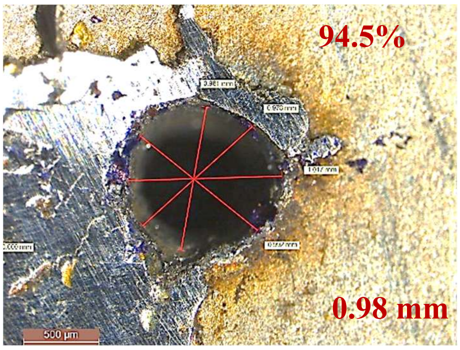

Fig. 3.8: Closure view of laser drilled hole top side.

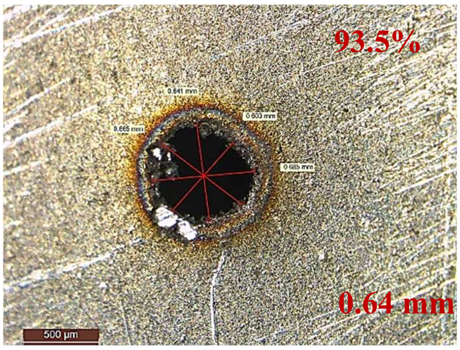

Fig. 3.9: Closure view of laser drilled hole bottom side.

3.4 **Taguchi method:** The Taguchi method [21-23] focuses on minimizing process variation through the robust design of experiments. The primary aim of this method is to produce high-quality products at a low manufacturing cost. Dr. Genichi Taguchi from Japan developed this method, emphasizing the significance of variation. He created a systematic approach to designing experiments to explore how various parameters influence both the mean and variance of a process performance characteristic that indicates the effectiveness of the process. Taguchi's proposed experimental design utilizes orthogonal arrays to structure the parameters impacting the process and the levels at which they should be modified. Rather than testing every possible combination as in factorial design, the Taguchi method evaluates pairs of combinations. This approach facilitates the gathering of essential data to identify which factors most significantly influence product quality while minimizing experimentation, thereby conserving time and resources. The Taguchi method is most effective when dealing with an intermediate number of variables (between 3 and 50), limited interactions among variables, and when only a small number of variables have a considerable impact. The Taguchi method has been adapted [24] by introducing a frequency-dependent level graph, enhancing the accurate prediction and design of specific frequency responses for spiral cavity absorbers. Benjamin D. Cobb and John M. Clarkson [25] have applied the modified Taguchi method to optimize polymerase chain reactions. Z. D. Zaharis [26] employed the modified Taguchi method for beamforming applications. In this study, we have implemented Taguchi method-based mean variance modelling to minimize hole diameter and taper angle while maximizing reproducibility. Taguchi arrays can be either derived or referenced. Smaller arrays can be created manually, while larger arrays can be generated using deterministic algorithms. In general, these arrays are accessible online. The selection of arrays is based on the number of parameters (variables) and the number of levels (states). In the following section, the detailed procedures for implementing the Taguchi method will be outlined.

The basic procedures associated with the Taguchi Method include the following:

1. Establish the objective of the process or, more specifically, define a target value for a performance measure relevant to the process. This could involve aspects like flow rate or temperature. Additionally, the process goal might represent a minimum or maximum; for instance, the aim could be to maximize the output flow rate. The deviation of the performance characteristic from the target value is utilized to formulate the loss function for the process.

2. Identify the design parameters that influence the process. These parameters are the controllable variables within the process that impact the performance measure, such as temperatures, pressures, etc. It is essential to specify the number of levels at which these parameters will be varied. For example, a temperature could be adjusted to low and high values of 40°C and 80°C. Increasing the number of levels for parameter variation leads to a greater number of experiments that need to be performed.

3. Develop orthogonal arrays for the parameter design, detailing the number of experiments and their conditions. The choice of orthogonal arrays is determined by the number of parameters and the levels of variation for each parameter, which will be explained further.

4. Execute the experiments as indicated in the completed array to gather data regarding their impact on the performance measure.

5. Perform data analysis to assess the influence of the various parameters on the performance measure.

Determining parameter design orthogonal array:

The influence of various parameters on performance characteristics can be assessed through a condensed series of experiments utilizing the orthogonal array experimental design introduced by Taguchi. After identifying the controllable parameters that impact a process, it is essential to determine the varying levels for these parameters. Establishing the levels for a variable requires a comprehensive understanding of the process, including the parameter's minimum, maximum, and current values. When there is a significant difference between a parameter's minimum and maximum values, the test values can either be separated further or more values can be included. Conversely, if the parameter's range is narrow, fewer values can be tested or the tested values can be closer together. For instance, if the operating temperature of a reactor jacket can range from 20 to 80 °C, and the current jacket temperature is known to be 50 °C, three levels might be selected at 20, 50, and 80 °C. Additionally, the costs associated with conducting experiments must be factored in when deciding on the number of parameter levels to include in the experimental design. In the previously mentioned jacket temperature example, conducting 60 levels at 1 °C intervals would be financially impractical. Generally, the same number of levels is selected for all parameters in the experimental design to facilitate the choice of the appropriate orthogonal array.

With the number of parameters and their corresponding levels known, the suitable orthogonal array can be identified. By consulting the array selector table provided below, the correct array name can be found by identifying the column and row that correspond to the number of parameters and levels. Once this name has been established (with the subscript indicating the number of experiments required), the predefined array can be referenced. These arrays were developed using an algorithm created by Taguchi, which ensures each variable and setting is tested consistently. For example, if there are three parameters (voltage, temperature, pressure) and two levels (high, low), the appropriate array is L4.

Table 1: Selection of orthogonal array.

		No. of parameters								
No. of Levels		**2**	**3**	**4**	**5**	**6**	**7**	**8**	**9**	**10**
	2	L_4	L_4	L_8	L_8	L_8	L_8	L_{12}	L_{12}	L_{12}
	3	L_9	L_9	L_9	L_{18}	L_{18}	L_{18}	L_{18}	L_{27}	L_{27}
	4	L_{16}	L_{16}	L_{16}	L_{16}	L_{32}	L_{32}	L_{32}	L_{32}	L_{32}
	5	L_{25}	L_{25}	L_{25}	L_{25}	L_{25}	L_{50}	L_{50}	L_{50}	L_{50}

Evaluating the experimental findings:

After establishing the experimental design and conducting the trials, the performance metrics obtained from each trial can be utilized to evaluate the comparative influence of the various parameters.

3.5 **Optimization of laser drilling process:** To optimize the laser drilling process, five parameters were chosen, including repetition rate, compressed air-assisted gas pressure, pulse width, number of pulses, and laser peak power. These parameters were modified at four distinct levels, and the effect of each individual parameter on cutting performance was analysed using the Taguchi method. An L_{16} array was utilized, based on the four process parameters and their four levels. The aim was to improve hole circularity while reducing taper angle and ensuring greater reproducibility. The experiment was performed on a 3 mm thick SS316 sheet, and hole diameter was assessed using an optical microscope.

Table 2: Factors and levels.

Factors (Parameters)	Level 1	Level 2	Level 3	Level 4
No. of pulses	40	50	60	70
Pulse width (ms)	4	5	6	7
Repetition rate (Hz)	4	5	6	7
Peak power (kW)	4.19	4.44	4.68	4.94
Assist gas pressure (Kg/cm^2)	7	8	9	10

Table 3: L_{16} Taguchi orthogonal array.

Experiment no.	No. of pulses	Pulse width	Repetition rate	Peak power	Gas pressure
1	1	1	1	1	1
2	1	2	2	2	2
3	1	3	3	3	3
4	1	4	4	4	4
5	2	1	2	3	4
6	2	2	1	4	3
7	2	3	4	1	2
8	2	4	3	2	1
9	3	1	3	4	2
10	3	2	4	3	1
11	3	3	1	2	4
12	3	4	2	1	3
13	4	1	4	2	3
14	4	2	3	1	4
15	4	3	2	4	1
16	4	4	1	3	2

3.5.1 **Maximization of hole circularity**

Taguchi proposes converting the output data from repeated trials into a unified value known as the S/N ratio. In this context, the ‘signal’ refers to the preferred value, while the ‘noise’ indicates the undesirable value. The signal-to-noise ratio reflects the variation around the target value.

For maximization, S/N ratio is

$$\mathrm{SN} = -10\log_{10}[\frac{1}{n}\sum_{i=1}^{n}\frac{1}{y_i^2}] \qquad [20]$$

Where, y_i = observed data (or quality characteristics) at i^{th} trial,

i = trial number and n = number of trials

Table 4: Experimental data for maximum hole circularity.

Experiment No.	Parameters					Hole circularity (%)		
	No. of pulses	Pulse width(ms)	Repetition rate (HZ)	Peak power(kW)	Gas pressure(kg/cm^2)	Trial 1	Trial 2	Trial3
1	40	4	4	4.19	7	84.21	85.22	92.31
2	40	5	5	4.44	8	94.49	91.01	90.77
3	40	6	6	4.68	9	95.03	94.38	90.51
4	40	7	7	4.94	10	91.08	90.63	89.81
5	50	4	5	4.68	10	90.84	85.93	94.15
6	50	5	4	4.94	9	86.78	90.41	91.28
7	50	6	7	4.19	8	92.08	94.99	93.62
8	50	7	6	4.44	7	93.15	92.03	90.64
9	60	4	6	4.94	8	92.45	93.65	93.91
10	60	5	7	4.68	7	94.21	88.72	93.94
11	60	6	4	4.44	10	88.42	90.08	89.08
12	60	7	5	4.19	9	94.91	91.47	91.26
13	70	4	7	4.44	9	84.05	93.11	92.91
14	70	5	6	4.19	10	93.47	89.85	93.61
15	70	6	5	4.94	7	96.21	92.04	93.35
16	70	7	4	4.68	8	91.37	98.01	84.37

Table 5: Experimental levels and data analysis for Table 4.

Experiment No.	Parameters					Avg. hole circularity (%)	SN value
	No. of pulses	Pulse width(ms)	Repetition rate (HZ)	Peak power(kW)	Gas pressure(kg/cm^2)		
1	1	1	1	1	1	87.24	38.79
2	1	2	2	2	2	92.09	39.28
3	1	3	3	3	3	93.31	39.39
4	1	4	4	4	4	90.51	39.13
5	2	1	2	3	4	90.31	39.10
6	2	2	1	4	3	89.49	39.03
7	2	3	4	1	2	93.56	39.42
8	2	4	3	2	1	91.94	39.27
9	3	1	3	4	2	93.33	39.40
10	3	2	4	3	1	92.29	39.29
11	3	3	1	2	4	89.19	39.01
12	3	4	2	1	3	92.54	39.32
13	4	1	4	2	3	90.02	39.06
14	4	2	3	1	4	92.31	39.30
15	4	3	2	4	1	93.87	39.45
16	4	4	1	3	2	91.25	39.16

Maximum hole circularity calculation for parameter 1 and for each level i.e. 4 levels

$$SN_{1,1}= \frac{38.79 + 39.28 + 39.39 + 3\ \ .13}{4} = 39.15$$

$$SN_{1,2}= \frac{39.10 + 39.03 + 39.42 + 39.27}{4} = 39.21$$

$$SN_{1,3}= \frac{39.40 + 39.29 + 39.01 + 39.32}{4} = 39.26$$

$$SN_{1,4}= \frac{39.06 + 39.30 + 39.45 + 39.16}{4} = 39.24$$

Maximum hole circularity calculation for parameter 2 and for each level i.e. 4 levels

$$SN_{2,1}= \frac{38.79 + 39.10 + 39.40 + 39.06}{4} = 39.09$$

$$SN_{2,2}= \frac{39.28 + 39.03 + 39.29 + 39.30}{4} = 39.23$$

$$SN_{2,3}= \frac{39.39 + 39.42 + 39.01 + 39.45}{4} = 39.32$$

$$SN_{2,4}= \frac{39.13 + 39.27 + 39.32 + 39.16}{4} = 39.22$$

Maximum hole circularity calculation for parameter 3 and for each level i.e. 4 levels

$$SN_{3,1}= \frac{38.79 + 39.03 + 39.01 + 39.16}{4} = 39.00$$

$$SN_{3,2}= \frac{39.28 + 39.10 + 39.32 + 39.45}{4} = 39.29$$

$$SN_{3,3}= \frac{39.39 + 39.27 + 39.40 + 39.30}{4} = 39.34$$

$$SN_{3,4}= \frac{39.13 + 39.42 + 39.29 + 39.06}{4} = 39.23$$

Maximum hole circularity calculation for parameter 4 and for each level i.e. 4 levels

$$SN_{4,1}= \frac{38.79 + 39.42 + 39.32 + 39.30}{4} = 39.21$$

$$SN_{4,2}= \frac{39.28 + 39.27 + 39.01 + 39.06}{4} = 39.16$$

$$SN_{4,3}= \frac{39.39 + 39.10 + 39.29 + 39.16}{4} = 39.24$$

$$SN_{4,4}= \frac{39.13 + 39.03 + 39.40 + 39.45}{4} = 39.25$$

Maximum hole circularity calculation for parameter 5 and for each level i.e. 4 levels

$$SN_{5,1}= \frac{38.79 + 39.27 + 39.29 + 39.45}{4} = 39.20$$

$$SN_{5,2}= \frac{39.28 + 39.42 + 39.40 + 39.16}{4} = 39.32$$

$$SN_{5,3}= \frac{39.39 + 39.03 + 39.32 + 39.06}{4} = 39.20$$

$$SN_{5,4}= \frac{39.13 + 39.10 + 39.01 + 39.30}{4} = 39.14$$

Table 6: Mean S/N value for each level and factor for maximum hole circularity.

Level	No. of pulses	Pulse width(ms)	Repetition rate (Hz)	Peak power(kW)	Gas pressure(kg/cm^2)
1	39.15	39.09	39.00	39.21	39.20
2	39.21	39.23	39.29	39.16	39.32
3	39.26	39.32	39.34	39.24	39.20
4	39.24	39.22	39.23	39.25	39.14
Δ	0.11	0.23	0.34	0.09	0.18
Rank	4	2	1	5	3

Results and discussion:

In the Taguchi method of optimization, a greater S/N value corresponds to a better performance regardless of the category of the performance characteristics. Therefore, the optimal level of the drilling parameters for all the parameters is the level with the greatest SN value. A quick review of the results in Table 6 reveals that the variation in the SN value with the change of parameters is the maximum for the repetition rate, followed by pulse width, assist gas pressure and number of pulses and it is the least for peak power. Hence, the repetition rate is the most dominant parameters for the range of parameters under investigation.

No. of pulses:

The effect of parameter number of pulses on hole circularity value in terms of S/N ratio is presented in Figure 3.10.

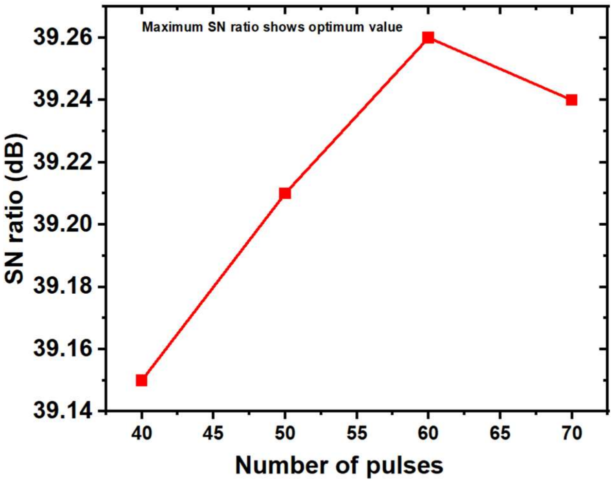

Fig. 3.10: S/N ratio vs number of pulses.

The graph of S/N ratio versus the number of pulses shows an increasing trend from 40 to 60 pulses, indicating that the signal-to-noise (S/N) ratio improves with the increase in pulse count within this range. However, at 70 pulses, the S/N ratio decreases, suggesting that beyond a certain threshold, increasing the number of pulses may lead to diminishing returns or potential degradation in signal quality. Therefore, the optimal number of pulses for achieving a high S/N ratio appears to be around 60.

Pulse width:

The effect of parameter pulse width on hole circularity value in terms of S/N ratio is presented in Figure 3.11.

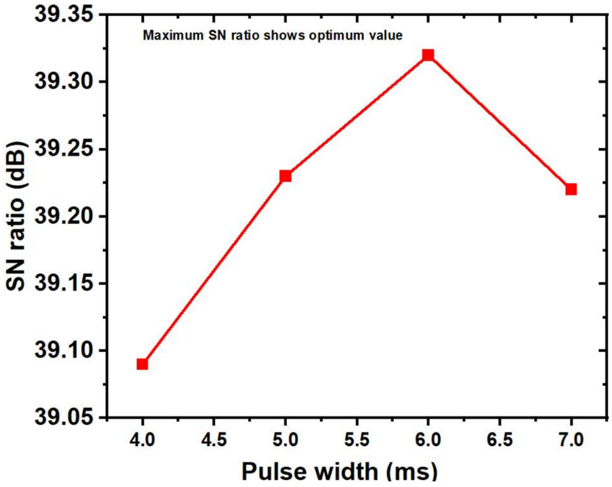

Fig. 3.11: S/N ratio vs pulse.

The graph shows that the S/N ratio initially increases with pulse width, reaching its peak at 6 ms, indicating that signal clarity improves as pulse width increases up to this point. However, beyond 6 ms, specifically at 7 ms, the S/N ratio decreases, suggesting a decline in signal quality. This implies that 6 ms is the optimal pulse width for maximizing the S/N ratio in the given system or experiment. Further increases in pulse width beyond this point may introduce more noise or reduce signal efficiency.

Repetition rate:

The effect of parameter repetition rate on hole circularity value in terms of S/N ratio is presented in Figure 3.12. The graph shows that the S/N ratio increases with repetition rate from 4 Hz to 6 Hz, indicating improved signal quality within this range. However, at 7 Hz, the S/N ratio decreases, suggesting a reduction in signal clarity or an increase in noise. This trend indicates that a repetition rate of 6 Hz is optimal for achieving the highest S/N ratio in the current setup. Repetition rates beyond this point may negatively impact signal performance.

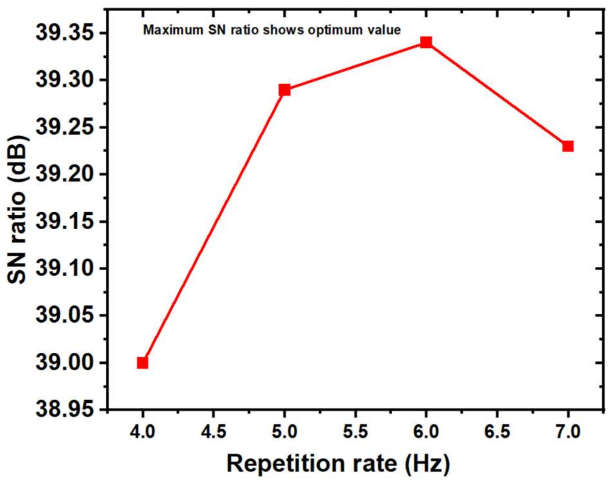

Fig. 3.12: S/N ratio vs repetition rate.

Peak power:

The effect of parameter peak power on hole circularity value in terms of S/N ratio is presented in Figure 3.13.

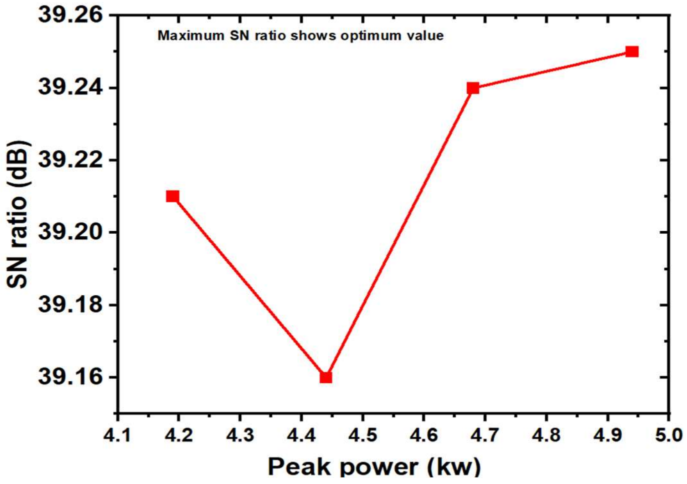

Fig. 3.13: S/N ratio vs peak power.

The graph shows that the S/N ratio decreases as peak power increases from 4.19 kW to 4.44 kW, indicating reduced signal quality in this range. However, beyond 4.44 kW, the S/N ratio increases steadily, reaching its maximum at 4.94 kW. This suggests that 4.94 kW is the optimal peak power for achieving the highest S/N ratio in the system. The initial drop may be due to transient effects or system non-linearity, while the subsequent rise reflects improved signal strength relative to noise at higher peak powers.

Assist gas pressure:

The effect of parameter assist gas on hole circularity value in terms of S/N ratio is presented in Figure 3.14.

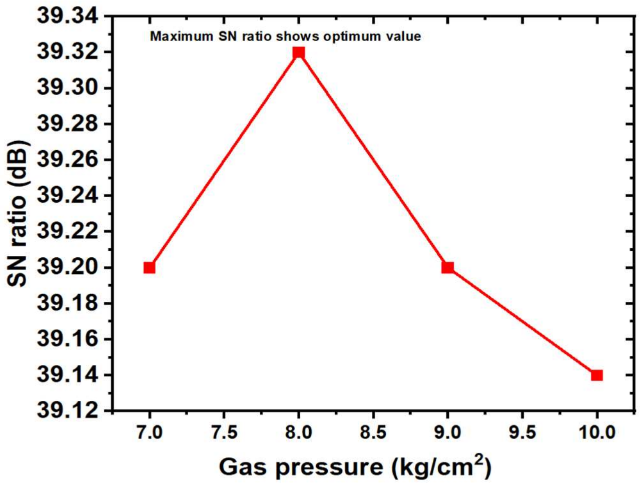

Fig. 3.14: S/N ratio vs assist gas pressure.

The S/N ratio increases as the assist gas pressure rises from 7 kg/cm² to 8 kg/cm², indicating improved signal quality in this range. However, beyond 8 kg/cm², the S/N ratio begins to decrease as the pressure increases up to 10 kg/cm². This suggests that 8 kg/cm² is the optimal assist gas pressure for maximizing the S/N ratio. Higher pressures beyond this point may introduce turbulence or instability, leading to increased noise or signal degradation.

3.5.2 **Minimization of taper angle of hole**

The approach used for minimization is

$$\mathrm{SN} = 10\log_{10}[\frac{1}{n}\sum_{i=1}^{n} y_i^2] \qquad [20]$$

Where, y_i = observed data (or quality characteristics) at i^{th} trial,

i = trial number and

n = number of trials

Taper angle:

$$\alpha = \tan^{-1}(\frac{\mathrm{D_f} - \mathrm{D_b}}{\mathrm{t}}) \qquad [27]$$

Where, α= Taper angle in degree

D_f = Front diameter, mm

D_b = Back diameter, mm

t = Thickness of the sample

Table 7: Experimental data for minimum taper angle.

Experiment No.	Parameters					Hole Taper angle (°)		
	No. of pulses	Pulse width(ms)	Repetition rate (HZ)	Peak power(kW)	Gas pressure (kg/cm^2)	Trial 1	Trial 2	Trial3
1	40	4	4	4.19	7	5.82	6.75	6.16
2	40	5	5	4.44	8	6.45	6.88	5.26
3	40	6	6	4.68	9	6.49	5.23	6.37
4	40	7	7	4.94	10	5.29	5.01	5.95
5	50	4	5	4.68	10	6.25	5.44	5.19
6	50	5	4	4.94	9	5.25	6.16	5.43
7	50	6	7	4.19	8	5.23	6.43	6.61
8	50	7	6	4.44	7	5.41	6.02	5.65
9	60	4	6	4.94	8	5.97	6.11	5.49
10	60	5	7	4.68	7	7.91	8.45	6.97
11	60	6	4	4.44	10	7.37	7.01	5.74
12	60	7	5	4.19	9	5.86	6.95	6.3
13	70	4	7	4.44	9	6.09	6.31	6.11
14	70	5	6	4.19	10	6.14	5.62	7.16
15	70	6	5	4.94	7	6.14	6.24	5.49
16	70	7	4	4.68	8	6.58	5.93	7.36

Table 8: Experimental levels and data analysis for Table 7.

Experiment No.	Parameters					Avg. hole taper angle (°)	SN value
	No. of pulses	Pulse width (ms)	Repetition rate (HZ)	Peak power (kW)	Gas pressure (kg/cm^2)		
1	1	1	1	1	1	6.24	15.92
2	1	2	2	2	2	6.19	15.90
3	1	3	3	3	3	6.03	15.64
4	1	4	4	4	4	5.42	14.70
5	2	1	2	3	4	5.63	15.03
6	2	2	1	4	3	5.61	15.01
7	2	3	4	1	2	6.09	15.74
8	2	4	3	2	1	5.69	15.12
9	3	1	3	4	2	5.86	15.36
10	3	2	4	3	1	7.77	17.84
11	3	3	1	2	4	6.71	16.58
12	3	4	2	1	3	6.37	16.10
13	4	1	4	2	3	6.17	15.81
14	4	2	3	1	4	6.31	16.04
15	4	3	2	4	1	5.96	15.51
16	4	4	1	3	2	6.62	16.46

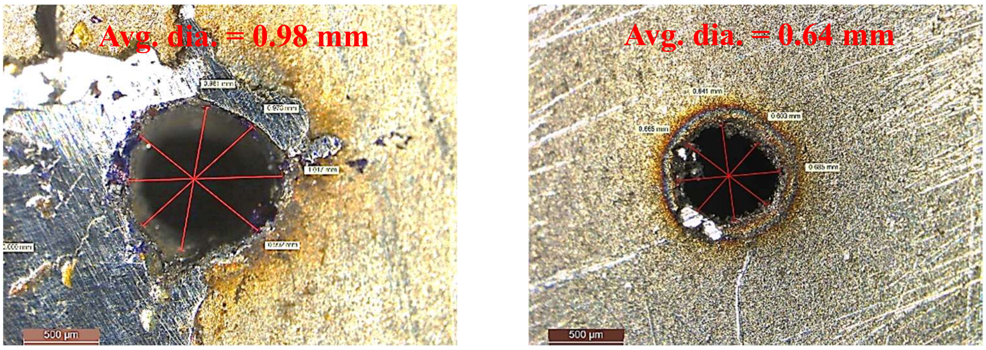

Fig. 3.15: Microscope image of front hole diameter and back hole diameter.

Minimum taper angle calculation for parameter 1 and for each level i.e. 4 levels

$$SN_{1,1}= \frac{15.92 + 15.90 + 15.64 + 14.70}{4} = 15.54$$

$$SN_{1,2}= \frac{15.03 + 15.01 + 15.74 + 14.12}{4} = 15.23$$

$$SN_{1,3}= \frac{15.36 + 17.84 + 16.58 + 16.10}{4} = 16.47$$

$$SN_{1,4}= \frac{15.81 + 16.04 + 15.51 + 16.46}{4} = 15.96$$

Minimum taper angle calculation for parameter 2 and for each level i.e. 4 levels

$$SN_{2,1}= \frac{15.92 + 15.03 + 15.36 + 15.81}{4} = 15.53$$

$$SN_{2,2}= \frac{15.90 + 15.01 + 17.81 + 16.04}{4} = 16.20$$

$$SN_{2,3}= \frac{15.64 + 15.74 + 16.58 + 15.51}{4} = 15.87$$

$$SN_{2,4}= \frac{14.70 + 15.12 + 16.10 + 16.46}{4} = 15.60$$

Minimum taper angle calculation for parameter 3 and for each level i.e. 4 levels

$$SN_{3,1}= \frac{15.92 + 15.01 + 16.58 + 16.46}{4} = 16.00$$

$$SN_{3,2}= \frac{15.90 + 15.03 + 16.10 + 15.51}{4} = 15.64$$

$$SN_{3,3}= \frac{15.64 + 15.12 + 15.36 + 16.04}{4} = 15.54$$

$$SN_{3,4}= \frac{14.70 + 15.74 + 17.84 + 15.81}{4} = 16.02$$

Minimum taper angle calculation for parameter 4 and for each level i.e. 4 levels

$$SN_{4,1}= \frac{15.92 + 15.74 + 16.10 + 16.04}{4} = 15.95$$

$$SN_{4,2}= \frac{15.90 + 15.12 + 16.58 + 15.81}{4} = 15.85$$

$$SN_{4,3}= \frac{15.64 + 15.03 + 17.84 + 16.46}{4} = 16.24$$

$$SN_{4,4}= \frac{14.70 + 15.01 + 15.36 + 15.51}{4} = 15.15$$

Minimum taper angle calculation for parameter 5 and for each level i.e. 4 levels

$$SN_{5,1} = \frac{15.92 + 15.12 + 17.84 + 15.51}{4} = 16.10$$

$$SN_{5,2} = \frac{15.90 + 15.74 + 15.36 + 16.46}{4} = 15.87$$

$$SN_{5,3} = \frac{15.64 + 15.01 + 16.10 + 15.81}{4} = 15.64$$

$$SN_{5,4} = \frac{14.70 + 15.03 + 16.58 + 16.04}{4} = 15.59$$

Table 9: Mean S/N value for each level and factor for minimum taper angle.

Level	No. of pulses	Pulse width(ms)	Repetition rate (Hz)	Peak power(kW)	Gas pressure(kg/cm^2)
1	15.54	15.53	16.00	15.95	16.10
2	15.23	16.20	15.64	15.85	15.87
3	16.47	15.87	15.54	16.24	15.64
4	15.96	15.60	16.02	15.15	15.59
Δ	1.24	0.67	0.48	1.09	0.51
Rank	1	3	5	2	4

Results and discussion:

In the Taguchi method of optimization, a greater S/N value corresponds to a better performance regardless of the category of the performance characteristics. Therefore, the optimal level of the drilling parameters for all the parameters is the level with the greatest S/N value. A quick review of the results in Table 9 reveals that the variation in the S/N value with the change of parameters is the maximum for the number of pulses, followed by peak power, pulse width, assist gas pressure and repetition rate and it is the least for repetition rate. Hence, the number of pulses is the most dominant parameters for the range of parameters under investigation.

No. of pulses:

Figure 3.16 displays how the number of pulses influences the hole taper angle in relation to the S/N ratio. The graph of SN ratio versus number of pulses indicates a fluctuating or zig-zag trend between 40 and 70 pulses. This irregular behaviour suggests variability in signal quality or noise levels within this pulse range, possibly due to system instability, external interference, or inherent limitations in signal processing during this interval. Further analysis may be required to identify and mitigate the source of these fluctuations to achieve a more stable SN ratio.

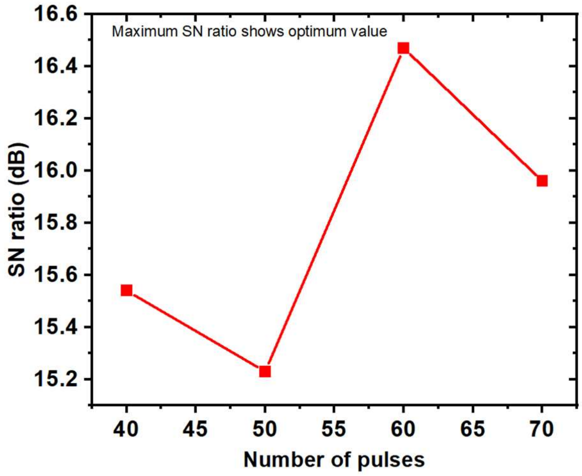

Fig. 3.16: S/N ratio vs number of pulses.

Pulse width:

Figure 3.17 displays how the pulse width of parameters influences the hole taper angle in relation to the S/N ratio. The S/N ratio increases from 4 ms to 5 ms, indicating improved signal quality or detection performance with increasing pulse duration up to 5 ms. However, beyond 5 ms (from 5 ms to 7 ms), the S/N ratio decreases, suggesting that extending the pulse duration further leads to a reduction in signal clarity or effectiveness. Therefore, a pulse duration of 5 ms appears to be the optimal point for maximizing the S/N ratio.

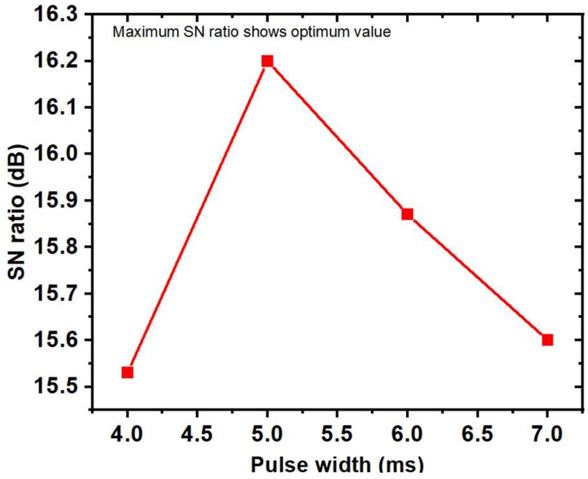

Fig. 3.17: S/N ratio vs pulse width.

Repetition rate:

Figure 3.18 displays how the repetition rate of parameters influences the hole taper angle in relation to the S/N ratio. The S/N ratio decreases gradually from 4 Hz to 6 Hz, indicating a potential decline in signal quality with increasing repetition rate in this range. However, a sudden increase in S/N ratio is observed at 7 Hz, corresponding to the through-hole point, suggesting a significant change in signal transmission or detection conditions. Notably, the S/N ratios at the initial (4 Hz) and final (7 Hz) points are approximately equal, implying an overall stable performance across the tested range despite intermediate fluctuations.

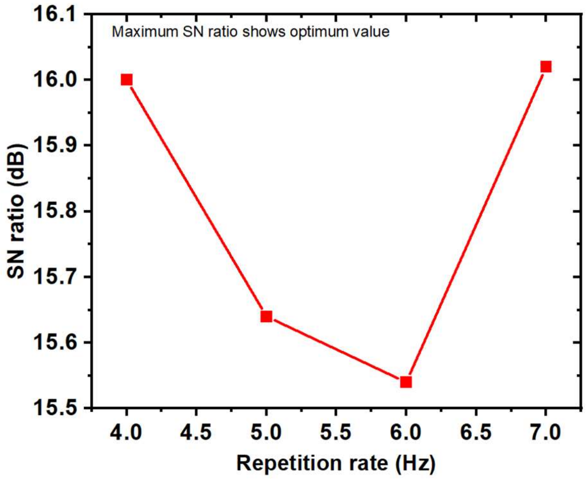

Fig. 3.18: S/N ratio vs repetition rate.

Peak power:

Figure 3.19 displays how the peak power of parameters influences the hole taper angle in relation to the S/N ratio.

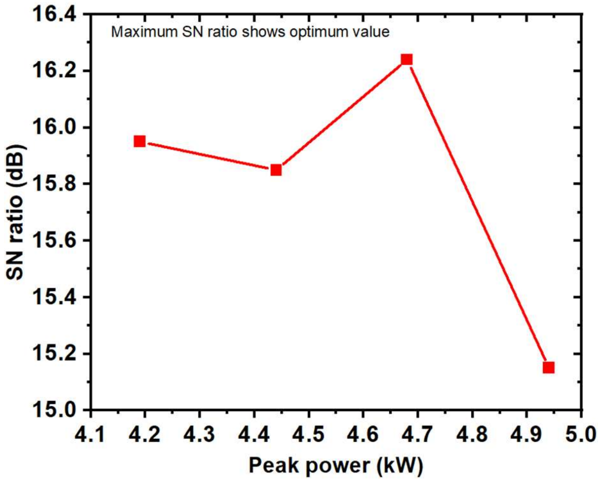

Fig. 3.19: S/N ratio vs peak power.

The graph of S/N ratio versus peak power shows that the S/N ratio reaches its maximum at 4.68 kW. This indicates that 4.68 kW is the optimal peak power level for achieving the highest signal quality relative to noise. Operating at this power level may ensure the most efficient signal transmission or detection in the system, while deviations from this point may lead to reduced S/N performance.

Assist gas pressure:

Figure 3.20 displays how the assist gas pressure of parameters influences the hole taper angle in relation to the S/N ratio.

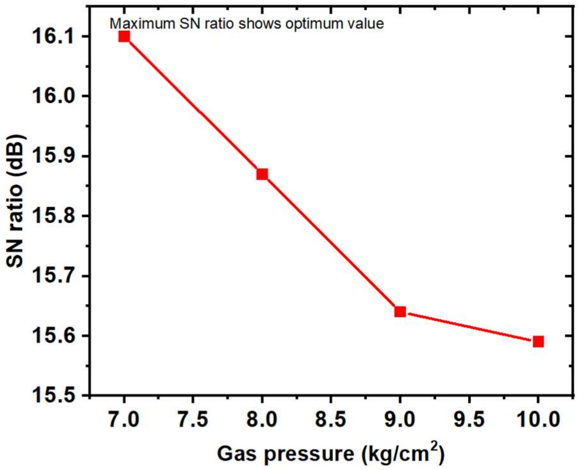

Fig. 3.20: S/N ratio vs assist gas pressure.

The S/N ratio increases with assist gas pressure and reaches its maximum at 7 kg/cm^2, indicating optimal signal quality at this pressure. Beyond 7 kg/cm^2, the S/N ratio begins to decrease, suggesting that higher gas pressures may introduce disturbances or reduce the effectiveness of signal transmission. Therefore, 7 kg/cm^2 appears to be the optimal assist gas pressure for maintaining the highest S/N ratio in the process.

Chapter 4

Theoretical Modeling

4.1 **Model description:** The laser beam strikes the surface of the workpiece, gets absorbed, and leads to heating, melting, and vaporization. The recoil pressure produced by surface vaporization, combined with the pressure from the assist gas, triggers the outward ejection of the liquid melt from the interaction area. Once a steady-state material removal is achieved, the drilling front moves into the material at a speed determined by the intensity of the absorbed laser. The model does not consider the initial ejection of the melt and focuses on the processes occurring once the drilled hole attains a certain depth. The total pressure responsible for melt ejection is the combination of the vapor pressure within the hole and the pressure applied to the melt by the assist gas. The accumulation of vapor pressure is alleviated by the escape of vapor through the drilled hole.

4.2 **Assumptions:** In the theoretical modeling, several assumptions have been considered to simplify the analysis. A steady-state material removal condition is assumed, with uniform laser intensity throughout the process. The variation in the radial direction of the hole is neglected, and the effects of radiation are not considered. It is further assumed that the melt vapor is ejected at sonic speed, and plasma generation during the process is considered negligible. Additionally, all the material that melts is assumed to be completely converted into oxide before being ejected from the melt surface.

4.3 **Aim of the model:** This study focuses on analysing the laser peak power required to achieve a desired drilling rate, as well as examining the influence of the melt surface temperature on the overall drilling efficiency. The objective is to determine the optimal peak power of the laser that ensures effective material removal while maintaining process stability and precision. A critical aspect of this analysis is understanding how variations in the melt surface temperature affect the rate at which material is removed. Therefore, the interplay between laser peak power and melt surface temperature is carefully studied to identify the operating conditions that yield the most efficient and controlled drilling performance.

4.4 **Mathematical formulation:**

4.4.1 Mass balance

Typically, throughout the drilling process, the speed at which the solid metal melts is equal to the rate at which material is extracted from the hole through both vaporization and the expulsion of melted material. This connection can be formulated mathematically to illustrate the conservation of mass during the drilling activity.

$$\frac{dm_s}{dt} = \frac{dm_v}{dt} + \frac{dm_m}{dt} \qquad (1)$$

Eq. (1) can be written as

$$\pi r_l^2 \rho_s V_d = \pi r_l^2 \rho_m V_v + 2\pi r_l \delta_m \rho_m V_m$$

Where m_s is the mass of solid metal melted, m_v is the mass of molten metal vapourised, m_m is mass of molten material ejected, r_l is laser beam radius, ρ_s is density of solid, V_d is drilling velocity along z-axis, ρ_m is density of melt, V_v is vaporization front velocity, δ_m is melt thickness and V_m is melt ejection velocity.

To calculate V_v , $V_v = V_0 \exp\left(\frac{-U}{T_s}\right)$ here $U = (M_A L_v)/(N_A k_b)$ (2)

M_A and L_v represent the atomic mass and the latent heat of vaporization of the metal, respectively. N_A denotes Avogadro's number, k_b signifies Boltzmann's constant, and V_0 is a constant that has a value approximately equal to the speed of sound in the condensed phase.

4.4.2 Melt ejection velocity

Given a consistent pressure distribution within the laser beam, this implies that the combination of vapor pressure and assist gas pressure results in a one-dimensional melt flow, with no pressure present beyond the beam. Therefore, it is possible to derive an equation for the melt velocity, V_m.

$$p_r + p_{eff} = \frac{\rho_m V_m^2}{2} \qquad (3)$$

Where p_r is recoil pressure and p_{eff} is assist gas effective pressure.

4.4.3 Vapour pressure

The vapor pressure can be directly determined using the well-established Clausius–Clapeyron equation.

$$p_{vap} = p_{atm} \exp\left[\frac{\Delta_{vap}H}{R}\left(\frac{1}{T_{vap}} - \frac{1}{T_s}\right)\right] - p_{atm} \qquad (4)$$

$$p_r = 0.5\, p_{vap} \qquad (5)$$

Where p_{vap} is vapour pressure, p_{atm} is atmospheric pressure, T_s is melt surface temperature, T_{vap} is temperature of vaporization, $\Delta_{vap}H$ is enthalpy of vaporization and R is gas constant.

4.4.4 Assist gas pressure

The pressure of assist gas at nozzle exit, p_g is defined as

$$p_g = \left(\frac{2}{\gamma+1}\right)^{\frac{\gamma}{\gamma-1}} p_n \tag{6}$$

Where p_n is the pressure inside the nozzle and γ is the specific heat ratio.

$$p_{eff} = p_n \frac{A_e}{A_e + A_r} \tag{7}$$

Where $A_e = \pi r_l^2$ is effective area of assist gas flow and $A_r = \pi d_n z_n$ is cylindrical area of radial loss assist gas pressure, d_n is nozzle exit diameter and z_n is stand of distance.

4.4.5 Drilling velocity

The total drilling velocity (V_d) is defined as the sum of the contributions from vaporization-induced drilling velocity and melt-ejection-induced drilling velocity within the interaction zone.

$$V_d = \frac{1}{2}\left\{\frac{\rho_m}{\rho_s}V_v + \left[\left(\frac{\rho_m}{\rho_s}V_v\right)^2 + 8\frac{\rho_m K_m}{\rho_s r_l}V_m\right]^{1/2}\right\} \tag{8}$$

Where K_m is thermal diffusivity of melt.

4.4.6 Energy balance

Based on the above equations, the absorbed laser intensity can be defined as the portion of the incident laser energy that is effectively transferred to the material within the interaction zone. This absorbed intensity accounts for energy contributions that lead to phase changes such as vaporization and melting and is a critical parameter in determining the efficiency and dynamics of the laser drilling process.

$$I_{abs} = [2\rho_m(C_m T^* + L_m)\frac{V_m K_m}{V_d r_l} + \rho_s C_s (T_m - T_0)V_d + \frac{\rho_s C_s (T_m - T_0) V_d}{\left(\frac{K_m}{K_s} + \frac{V_d}{K_s} r_l\right)^{1/2}} + \rho_m V_v L_v \tag{9}$$

Where I_{abs} = Absorbed laser intensity, $C_m$is Specific heat of liquid, K_s is Thermal diffusivity of solid, T^* is Avg. temperature, L_m is Latent heat of melt, L_v= Latent heat of vaporization, C_s is Specific heat of solid and T_m is Melt temperature of solid.

4.5 **Physical properties:** The physical properties taken for the solid stainless steel are given

$V_0 = 882\,\frac{\mathrm{m}}{\mathrm{s}}$, $T_{vap} = 3100$ K, $M_A = 0.05575\,\frac{\mathrm{Kg}}{\mathrm{mol}}$, $L_v = 6333000\,\frac{\mathrm{J}}{\mathrm{Kg}}$, $\rho_s = 7.8\,\frac{\mathrm{g}}{\mathrm{cm}^3}$, $\rho_m = 6.98\,\frac{\mathrm{g}}{\mathrm{cm}^3}$

$C_s = 0.628\,\frac{\mathrm{J}}{\mathrm{gK}}$, $C_m = 0.748\,\frac{\mathrm{J}}{\mathrm{gK}}$, $K_s = 0.14\,\frac{\mathrm{cm}^3}{\mathrm{s}}$, $K_m = 0.07\,\frac{\mathrm{cm}^3}{\mathrm{s}}$, and $L_m = 276\,\frac{\mathrm{J}}{\mathrm{g}}$

4.6 **Results and discussions:**

A theoretical mathematical model has been developed to study the laser peak power requirements necessary to achieve a target drilling rate, as well as to analyse the influence of melt surface temperature on the drilling performance. The model is based on a set of predefined process parameters to simulate realistic laser-material interaction conditions. Specifically, the laser beam radius was assumed to be 0.2 mm, with a nozzle exit diameter of 1.5 mm and a stand-off distance of 1.5 mm. Compressed air at a pressure of 10 kg/cm² was employed as the assist gas. A pulse width of 4 ms was selected to reflect typical pulsed laser operation. To assess the thermal influence on the drilling rate, the melt surface temperature was varied from 3100 K to 4200 K. Using these input parameters, the model was used to calculate the theoretical values of laser peak power and corresponding drilling rates. The results are presented in the Table 10, which provides a quantitative evaluation of the drilling process under different thermal conditions.

Table 10: Theoretical calculation at varying melt surface temperatures.

Sr. No.	T_s (K)	I_{abs} (MW/cm^2)	P_r (kg/cm^2)	V_m (m/s)	V_d (m/s)
1	3100	0.99	0.00	2.13	0.36
2	3200	1.27	0.27	3.51	0.47
3	3300	1.49	0.66	4.83	0.55
4	3400	1.71	0.12	6.21	0.62
5	3500	1.92	1.91	7.71	0.70
6	3600	2.13	2.89	9.34	0.77
7	3700	2.35	4.16	11.12	0.84
8	3800	2.58	5.81	13.07	0.91
9	3900	2.82	7.91	15.20	0.98
10	4000	3.06	10.53	17.51	1.05
11	4100	3.32	13.80	20.00	1.11
12	4200	3.59	17.81	22.68	1.19

Based on above Table 10 data Figure 4.1 shows the relation between absorbed laser beam intensity and melt surface temperature.

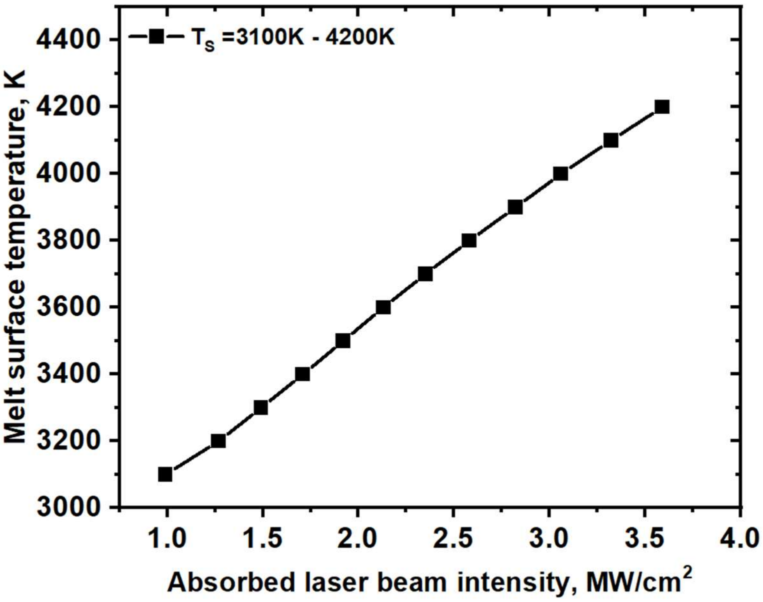

Fig. 4.1: Absorbed laser intensity vs melt surface temperature.

The graph illustrates the relationship between the absorbed laser beam intensity and the resulting melt surface temperature during the laser drilling process. As observed, the melt surface temperature increases consistently with the rise in absorbed laser intensity, ranging from approximately 3100 K to 4200 K for an intensity span of 1.0 MW/cm² to 3.7 MW/cm². This positive correlation indicates that higher absorbed laser energy leads to increased thermal input at the material surface, thereby elevating the surface temperature of the melt. This trend aligns with the fundamental principles of laser-material interaction, where greater energy absorption enhances the heating and phase transformation rates. The nearly linear nature of the curve suggests a proportional relationship within the studied range, which can be critical in determining the optimal laser parameters for controlled drilling and material removal efficiency.

Based on above tabulated Table 10 data Figure 4.2 shows the relation between absorbed laser beam intensity and melt ejection velocity. The graph presents the variation of melt ejection velocity as a function of absorbed laser beam intensity during the laser drilling process. It is evident that as the absorbed intensity increases from 1.0 MW/cm² to approximately 3.6 MW/cm², the melt ejection velocity rises significantly, ranging from about 2 m/s to over 22 m/s. This nonlinear, upward trend reflects the enhanced momentum transfer to the molten material at higher energy inputs. As more laser energy is absorbed, the melt pool reaches higher temperatures and generates increased vapor recoil pressure, leading to more forceful ejection of molten material from the interaction zone. The observed behaviour underscores the critical role of absorbed intensity in controlling melt dynamics and material removal efficiency in laser drilling. This relationship is particularly important in optimizing process parameters to improve drilling quality, reduce recast layers, and enhance overall precision.

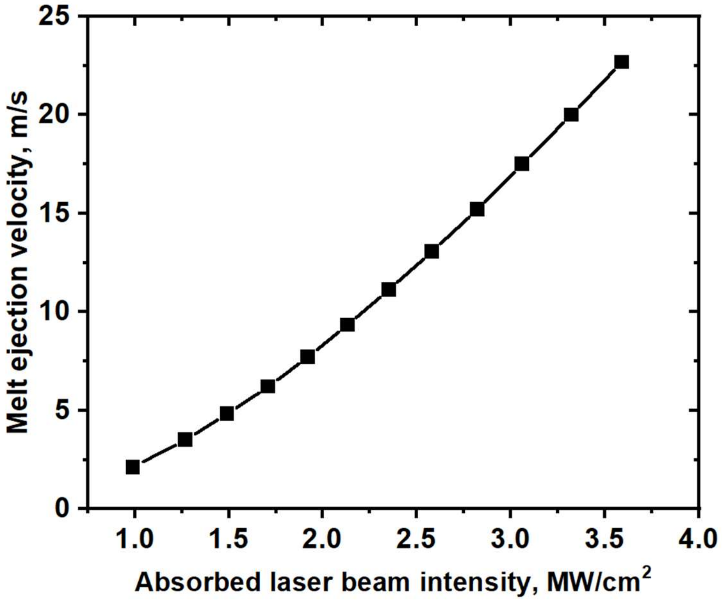

Fig. 4.2: Absorbed laser intensity vs melt ejection velocity.

Chapter 5

Experimental verification

5.1 **Experimental description:** To validate the theoretical model, an experimental investigation was conducted using a 3 mm thick sample of SS316 stainless steel. The laser source employed was a Fiber-coupled pulsed Nd: YAG laser system, configured to deliver a peak power of 5 kW, wavelength 1.06 µm and an average output power of 250 W. The laser beam was focused to a diameter of 400 µm on the workpiece surface. A single laser pulse with a pulse duration of 4 ms was used for each trial. Compressed air served as the assist gas to aid in molten material removal and was delivered through a nozzle with a fixed standoff distance of 1.5 mm from the workpiece surface. This experimental configuration was selected to closely replicate the conditions assumed in the theoretical model, enabling a direct comparison of predicted and observed drilling performance.

5.2 **Formulation and calculation:** During the experimental verification, a laser power meter was employed to measure average output power and the corresponding energy delivered in each pulse. The peak power of the laser was determined and subsequently divided by the beam spot area to calculate the absorbed laser beam intensity for each trial. This method enabled accurate quantification of the energy density incident on the material surface. The drilling velocity in each experiment was computed using the analytical expression provided in Equation 11, which correlates the material removal depth with the pulse duration. This approach allowed for a systematic evaluation of the relationship between absorbed laser intensity and the resulting drilling performance, facilitating a direct comparison with the theoretical predictions.

$$\text{Drill depth}=\frac{1}{2}\times V_d\times \text{pulse width} \tag{10}$$

Table 11: Experimental calculated data.

Sr. No.	Current (A)	Experimental I_{abs} (MW/cm^2)	Drill depth (mm)	V_d (m/s)
1	200	1.44	1.05	0.53
2	220	1.79	1.15	0.57
3	240	2.12	1.34	0.67
4	260	2.42	1.36	0.68
5	280	2.68	1.67	0.84
6	300	3.00	1.77	0.89

5.3 **Results and discussions:**

Figure 5.1 shows the comparison of theoretical modeling and experimental verification. The graph illustrates the variation of drilling velocity with respect to absorbed laser beam intensity, comparing theoretical predictions with experimental results. The data correspond to an assist gas pressure of 10 kg/cm². As shown, both the theoretical and experimental drilling velocities exhibit an increasing trend with higher absorbed laser intensities. The theoretical values (represented by square markers) demonstrate a consistent and near-linear increase, indicating the model's sensitivity to rising energy input.

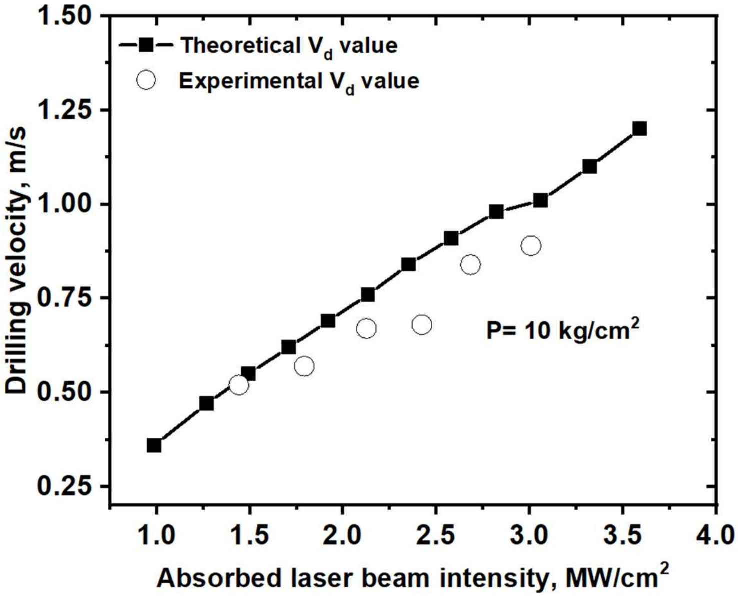

Fig. 5.1: Comparison of theoretical data with experimental data.

Experimental values (depicted by circular markers), while following a similar trend, lies below the theoretical curve. This discrepancy may be attributed to real-world losses such as imperfect energy absorption, heat conduction into the bulk material, and dynamic effects of molten material ejection. Notably, the experimental drilling velocities tend to level off slightly at higher intensities, possibly due to saturation effects or limitations in melt expulsion efficiency at elevated temperatures. Overall, the graph confirms the validity of the theoretical model in predicting drilling velocity trends, while also highlighting the influence of practical factors that must be considered during laser drilling operations. So, theoretical modeling is experimentally verified, and maximum error is found to be 15%.

Chapter 6

Conclusion

The thesis presents a comprehensive study on the theoretical modeling and experimental verification of the laser drilling process of SS316. The findings validate the proposed model and highlight the constraints and assumptions inherent in the theoretical framework, reinforcing confidence in its applicability. Overall, this work contributes valuable insights to the field of mechanical engineering and the optimization of laser drilling processes.

Experimental investigation provides a thorough exploration of laser-material interactions, detailing the absorption and reflection processes that influence the effectiveness of laser applications. The experimental investigations conducted on SS316 stainless steel highlight the significance of various parameters, such as pulse width, repetition rate, and gas pressure, in determining hole characteristics like circularity and taper angle. By employing optical microscopy and image processing techniques, this work establishes a solid foundation for understanding the complexities of laser drilling, paving the way for subsequent theoretical modeling and optimization efforts.

Theoretical modeling successfully outlines a one-dimensional theoretical model that predicts the depth of cut in single-pulse laser drilling operations, focusing on the mechanisms of material removal driven by vaporization. The model incorporates key assumptions, such as steady-state conditions and uniform laser intensity, while addressing the fluid dynamics of the molten flow. The theoretical framework established in this work serves as a foundation for further experimental validation and refinement, enhancing the understanding of laser drilling processes.

Experimental verification confirms the validity of the theoretical model through systematic experimental verification using SS316 stainless steel. The comparative analysis of drilling velocities reveals a consistent trend between theoretical predictions and experimental results, despite some discrepancies attributed to real-world factors. Overall, the findings reinforce the model's predictive accuracy, with a maximum error of 15%, and highlight the practical considerations necessary for optimizing laser drilling operations.

REFERENCES

[1] Steen, W. M., & Mazumder, J. (2010). *Laser material processing*. springer science & business media.

[2] Simpson, E. (2012). The basic principles of laser technology, uses and safety measures in anaesthesia anaesthesia tutorial of the week 255 19th march 2012.

[3] Mahan, A. I. (1965). Absorption, spontaneous emission, stimulated emission, and Maxwell's equations. *Journal of the Optical Society of America*, *55*(12), 1611-1616.

[4] Silfvast, W. T. (2004). *Laser fundamentals*. Cambridge university press.

[5] Endo, M., & Walter, R. F. (Eds.). (2018). *Gas lasers*. CRC Press.

[6] Koechner, W. (2013). *Solid-state laser engineering* (Vol. 1). springer.

[7] Keller, U., & Paschotta, R. (2021). *Ultrafast lasers*. Springer International Publishing

[8] Zhao, W., & Mei, X. (2021). Optimization of trepanning patterns for holes ablated using nanosecond pulse laser in Al2O3 ceramics substrate. *Materials*, *14*(14), 3834

[9] Jacobs, P. (2008, October). Precision trepanning with a fiber laser. In *ICALEO 2008: 27th International Congress on Laser Materials Processing, Laser Microprocessing and Nanomanufacturing*. AIP Publishing

[10] *Pattanayak, S., Panda, S., & Dhupal, D. (2020). Laser micro drilling of 316L stainless steel orthopedic implant: A study. Journal of Manufacturing Processes, 52, 220-234.*

[11] Zhao, J., Li, C., & Wang, J. (2023). Numerical simulation of nanosecond laser drilling of 316L stainless steel: addition of laser focus and analysis of manufacturing process. *Modelling and Simulation in Materials Science and Engineering*, *32*(1), 015009.

[12] Wang, X. D., Michalowski, A., Walter, D., Sommer, S., Kraus, M., Liu, J. S., & Dausinger, F. (2009). Laser drilling of stainless steel with nanosecond double-pulse. *Optics & Laser Technology*, *41*(2), 148-153.

[13] Chatterjee, S., Mahapatra, S. S., Sahu, A. K., Bhardwaj, V. K., Choubey, A., Upadhyay, B. N., & Bindra, K. S. (2018). Experimental investigation of quality characteristics in Nd: YAG laser drilling of stainless steel (AISI 316). *Materials Today: Proceedings*, *5*(5), 11526-11530.

[14] Chengal Reddy, V., Keerthi, T., Nishkala, T., & Maruthi Prasad Yadav, G. (2021). Analysis and optimization of laser drilling process during machining of AISI 303 material using grey relational analysis approach. *SN Applied Sciences*, *3*(3), 335.

[15] Wang, C., Wang, Q., Qian, Q., & Di, B. (2020, March). The development of laser drilling: A review. In *IOP Conference Series: Materials Science and Engineering* (Vol. 782, No. 2, p. 022067). IOP Publishing.

[16] Low, D. K. Y., Li, L., & Byrd, P. J. (2002). Hydrodynamic physical modeling of laser drilling. *J. Manuf. Sci. Eng.*, *124*(4), 852-862.

[17] Ng, G. K. L., Crouse, P. L., & Li, L. (2006). An analytical model for laser drilling incorporating effects of exothermic reaction, pulse width and hole geometry. *International Journal of Heat and Mass Transfer*, *49*(7-8), 1358-1374.

[18] Kaplan, A. F. (1996). An analytical model of metal cutting with a laser beam. *Journal of applied physics*, *79*(5), 2198-2208.

[19] Ghoreishi, M., Low, D. K. Y., & Li, L. (2002). Comparative statistical analysis of hole taper and circularity in laser percussion drilling. *International Journal of Machine Tools and Manufacture*, *42*(9), 985-995.

[20] Dubey, A. K., & Yadava, V. (2008). Robust parameter design and multi-objective optimization of laser beam cutting for aluminium alloy sheet. *The International Journal of Advanced Manufacturing Technology*, *38*, 268-277.

[21] Cimbala, J. M. (2014). Taguchi orthogonal arrays. *Pennsylvania State University*, 1-3.

[22] Mitra, A. (2011). The taguchi method. *Wiley Interdisciplinary Reviews: Computational Statistics*, *3*(5), 472-480.

[23] Milos, M., & Miroslav, R. (2013). Application of the Monte Carlo method for laser cutting optimization. *Revista de Tehnologii Neconventionale*, *17*(4), 46.

[24] MacDonald, A. D. (1990, May). A modified Taguchi method for the design of broadband spiral cavity absorbers. In *International Symposium on Antennas and Propagation Society, Merging Technologies for the 90's* (pp. 1180-1183). IEEE.

[25] Cobb, B. D., & CIarkson, J. M. (1994). A simple procedure for optimising the polymerase chain reaction (PCR) using modified Taguchi methods. *Nucleic acids research*, *22*(18), 3801-3805.

[26] Zaharis, Z. D. (2012). A modified Taguchi's optimization algorithm for beamforming applications. *Progress In Electromagnetics Research*, *127*, 553-569.

[27] Kovalenko, V., Anyakin, M., & Uno, Y. (2000). Modeling and Optimization of Laser Semiconductors Cutting. *Proceedings of the ICALEO, Laser Microfabrication*, *90*, 82-92.